Computational Fluid Dynamics for Civil Engineering Infrastructure

By

Eyosias Beneberu

BSc from Bahirdar University, Bahirdar Ethiopia

July 2007

Submitted to the Faculty of the
Graduate College of the
Oklahoma State University
in partial fulfillment of
the requirements for
the Degree of

MASTER OF SCIENCE

July, 2008

Computational Fluid Dynamics for Civil Engineering Infrastructure

Thesis Approved:

Dr. Jonathan S. Goode

Thesis Adviser

Dr. Bruce W. Russell,

Dr. Robert N. Emerson

Dr. A. Gordon Emslie

Dean of the Graduate College

ACKNOWLEDGMENTS

First of all I would like to thank God of my ancestors who has been a good father and a friend to me throughout the years. I could not have been here if it wasn't for his mercy and love.

This thesis could not have been written without Dr. Goode, who not only served as my advisor but also encouraged and challenged me throughout my academic program. He has also played a pivotal role in my understanding of structural dynamics, finite element, natural hazards and advanced mechanics of materials.

I would also like to thank Dr. Bruce Russell and Dr. Robert Emerson for serving as my graduation committee. Dr. Russell has been helpful in giving me the proper guidance and support. He also helped to gain the basic knowledge about pre stressed concrete. Dr. Emerson has been instrumental in developing my skills in structural analysis.

I must thank Dr. Tyler Ley who has shown me the quality of good professor. He has been instrumental in advancing my knowledge in the design of reinforced concrete and design of structural steel.

Lastly, I would like to thank my parents and extended family for all of their love, support, and encouragement. I could never have gotten here without them and I owe them the world.

TABLE OF CONTENTS

LIST OF TABLES

Table Page

LIST OF FIGURES

Figure Page

CHAPTER I

INTRODUCTION

1.1 Overview of Computational Fluid Dynamics (CFD)

Fluid (gas and liquid) flows are governed by partial differential equations which represent conservation laws for mass, momentum, and energy. Computational fluid dynamics (CFD) is the method of replacing these partial differential equations system by a set of algebraic equations which can be solved by a digital computer.

CFD has been used in many areas of science including aerodynamics of aircraft and cars, hydrodynamics of ships, pumps and turbines, and combustion and heat transfer in chemical engineering. It also has a diverse application in civil engineering such as wind loading on structures, wind and wave power, ventilation, fire and explosion hazards, dispersion of pollutants and effluent, wave loading on coastal and offshore structures, hydraulic structures, sediment transport, and hydrology. Other applications include weather forecasting, plasma physics, blood flow, and heat dissipation from electronic circuitry.

CFD gives an insight into flow patterns that are difficult or impossible to study using traditional (experimental) techniques. It has the advantages over experimental simulations in such a way that it is cheaper, faster, and multipurpose. Also, CFD software is portable and easy to use and modify. However, the results of CFD simulation are rarely 100% reliable because the input data may involve overly simplified assumptions such that the mathematical model at hand may be inadequate. Furthermore, the accuracy of the result is also limited by the available computing power.

All CFD codes, or software, have three main elements: (i) a Pre-Processor (ii) a Solver and (iii) a Post-Processor.

Pre-Processor

Pre-Processing involves the input of the flow problem into a CFD program by a means of a user-friendly interface and subsequent transformation of this input into a form suitable for use by the solver. The Pre-Processing stage includes:

- Definition of the computational domain or the geometry of the region of interest,
- Generation of mesh or sub-dividing the computational domain into smaller pieces,

- Selection of the chemical and physical phenomena that needs to be modeled,
- Assigning fluid properties, and
- Defining the boundary conditions.

Predominately, the accuracy of a CFD solution depends on the number of cells in the grid. In general, the larger the number of cells (fine mesh), the better the accuracy of the solution. But using a fine mesh can be computationally expensive because it requires a large capacity computer and can take substantial time for an analysis. An optimal mesh is recommended to solve any particular problem. An optimal mesh is often non-uniform, finer in areas where large variations occur from point to point and coarser in regions with relatively little change.

Solver

The Solver involves discretization or conversion of the governing partial differential equations of fluid flow into a system of algebraic equations and then solving them iteratively to get the flow variables (pressure, velocity, temperature, etc.).

Post-Processor

The Post-Processing stage involves visualization of analysis result. The Post-Processor in CFD software has the capacity of generating graphics for:

- Line and shaded contour plots of pressure,
- Vector plots,
- 2D and 3D surface plots,
- Surface streamlines, and
- Animation, among others.

1.2 Sign Support Structures

Sign support structures are found on many major highways around the world. They help the highway user in giving the proper directions and important information. The signage consists of either aluminum signs or variable message signs (VMS). The complexity of sign support structures range from a single pole cantilever to four chord truss structures that span several lanes of traffic.

The cantilever sign support structure is made from horizontal and vertical components. The horizontal component is known as the mast arm (usually in reference to a monotube, i.e. single tube without joints), the truss (for other than the monotube), or the cantilever. The vertical column is known as upright posts or poles.

In the fourth edition of the *Standard Specifications for Structural Supports for Highway Signs, Luminaries, and Traffic Signals* (AASHTO, 2001), structures supported on both sides of the roadway are referred to as bridge supports. Bridge supports are also called

span-type structures, sign bridges, or overhead structures, although this latter term is sometimes used to describe both cantilever and bridge supports (Dexter and Ricker, 2002). The vertical members that support the mast can be a single pole, box-truss structure, etc.

According to NCHRP (National Cooperative Highway Research Program) Report 469 (2002), cantilevered support structures are a good choice because the cost is typically less than 40 percent of the cost of bridge supports. Also, the single upright increases motorist safety by reducing the probability of vehicle collision. But, the single support has a greater tendency of increasing the flexibility of the cantilevered structure. Figure 1-1 illustrates a typical cantilever sign support structure.

Figure 1-1: Cantilever sign support structure

The length of the horizontal mast arm of the cantilever sign support structure has increased in the past years which results in an increase in flexibility. States Departments of Transportation (DOT) have increased the span for two reasons. First, the set back distance of the column from the roadway is increased. Second, DOTs have to increase the length as these structures are being used on roads with many more lanes.

The increase in flexibility as well as low mass results in a very low resonant frequency of about 1Hz for these structures. The critical damping is extremely low with a value

usually less than 1%. These result in conditions that make cantilever support structures vulnerable to large amplitude vibrations and fatigue cracking caused by wind-loading.

An example failure of a cantilevered supported structure is one that happened on July 7, 2008 on I-65 in Tennessee. As it is seen in Figure 1-2, the sign support fell on to the highway because of the failure at the base of the pole. Early investigation by the Tennessee DOT showed that prolonged exposure to wind created by tractor trailer gusts may have contributed to the problem (WSMV, 2008).

Figure 1-2: Failure of cantilever sign support structure along I-65 in Tennessee

To prevent large amplitude vibration and development of fatigue cracks in cantilever and non-cantilevered structures, the American Association of State Highway and Transportation Officials (AASHTO) lists four types of wind fatigue design loads in the 2001 *Standard Specifications for Structural Supports for Highway Signs, Luminaries and Traffic Signals*. These loads are galloping, vortex shedding, natural wind gusts, and truck induced gusts.

1.3 Research Objective

The research has three main objectives. The first objective is to develop the theoretical background of CFD. The second objective is to compare the result of wind fatigue design load on cantilever sign support structure specifically for natural wind gust using computational fluid dynamics (CFD) with the result from the AASHTO provision which

is derived by considering the yearly mean wind speed. The final objective is to show the application of CFD in civil engineering. This is done by:

1. Developing the theoretical background for CFD,
2. Analyzing the sign support structure by using a CFD software, ANSYS-CFX, to get the pressure,
3. Calculate the pressure on the sign support by using the AASHTO provision for natural wind gust,
4. Analyze the structure using finite element software, STAAD, to calculate the stresses due to the pressure from CFD analysis and AASHTO provision, and
5. Compare the stresses from the CFD analysis and AASHTO provision.

1.4 Thesis Organization

The thesis is organized into 5 chapters. Chapter 2 presents the theoretical background of CFD. This includes the governing differential equations of fluid flow, numerical discretization, solution algorithm for the Navier-Stokes equation in both steady and unsteady flow, types of grids and convergence. It also gives background information about the ANSYS-CFX CFD software. Chapter 3 outlines the specifications of AASHTO in relation to sign support structures. Chapter 4 presents the pressure and stress analysis for both the AASHTO provision and ANSYS-CFX CFD analysis. Lastly, Chapter 5 summarizes the results from Chapter 4 and presents conclusions and recommendations.

CHAPTER II

MATHEMATICAL FORMULATION

2.1 Governing Differential Equations

The equations governing the fluid motion are derived based on the three fundamental principles of mass, momentum and energy conservation. These equations are continuity, momentum and energy.

A continuity equation describes the conservative transport of some kind of quantity. The general form of the continuity equation is:

$$\frac{\partial \phi}{\partial t} + \nabla . f = s \tag{2.1}$$

where $\boldsymbol{\phi}$ is some quantity, f is the function describing the flux of $\boldsymbol{\phi}$ and s describes the generation or removal rate of $\boldsymbol{\phi}$.

In fluid dynamics, the continuity equation is a mathematical statement that states the rate at which a mass enters the system is equal to the rate at which the mass leaves the system. The differential form of the continuity equation for fluids is given by:

$$\frac{\partial \rho}{\partial t} + \nabla(\rho u) = 0 \tag{2.2}$$

ρ is the fluid density, t is the time, and u is the fluid velocity. If the density is constant, as in the case of an incompressible flow, the mass continuity equation simplifies to a volume continuity equation as:

$$\nabla . U = 0 \tag{2.3}$$

The second type of equation that is used to describe fluid flow is the momentum equation. It is derived based on Newton's second law of motion which is given by:

$$\rho \frac{DV}{Dt} = \nabla \zeta_{ij} - \nabla p + \rho F \tag{2.4}$$

where V is the fluid velocity vector, ζ_{ij} is the viscous stress, P is the pressure, and F is the body force. If the fluid is incompressible and the coefficient of viscosity, μ, is constant then the momentum equation simplifies to:

$$\rho \frac{DV}{Dt} = \mu\nabla^2 \mathrm{V} - \nabla \mathrm{p} + \rho F \tag{2.5}$$

In situations where the fluid may be treated as incompressible and temperature differences are small, the continuity and momentum equations are sufficient to specify the velocity and pressure. But if heat flux occurs (temperature is not constant), at least one additional equation is required. In such a case, the energy equation is used. The energy equation is derived based on the first law of thermodynamics. The first law of thermodynamics states that energy can be transformed (changed from one form to another) but it can neither be created nor destroyed. In other words, the total energy of the system is conserved. The energy equation can be expressed mathematically as:

$$\rho \frac{De}{Dt} + \rho(\nabla . V) = \frac{\partial Q}{\partial t} - \nabla . q + \Phi \tag{2.6}$$

where Q is the heat source term, Φ is the dissipation term, $\nabla . q$ is the heat loss by conduction, and e is the internal energy. q can be expressed as:

$$q = -k\nabla T \tag{2.7}$$

where k is the coefficient of thermal conductivity, and T is the temperature. If the fluid is incompressible and the coefficient of viscosity of the fluid, μ, and the coefficient of thermal conductivity, k, are constant, the equation reduces to:

$$\rho \frac{De}{Dt} = \frac{\partial Q}{\partial t} + k\nabla^2 T + \Phi \tag{2.8}$$

For this study it is assumed that fluids are incompressible and the temperature difference is very small. As a result, the momentum and the continuity equation suffice to solve for the pressure and velocity (i.e., the energy equation is not needed).

2.2 Navier–Stokes Equations

The momentum equation together with the continuity equation makes up the Navier-Stokes equations to describe the flow of incompressible Newtonian fluids. It is used to describe the motion or flow of either liquids or gases.

The momentum equation in the Cartesian coordinate system can be expressed as:

X direction:

$$\rho\left(\frac{\partial u}{\partial t} + u\frac{\partial u}{\partial x} + v\frac{\partial u}{\partial y} + w\frac{\partial u}{\partial z}\right) = -\frac{\partial p}{\partial x} + \mu\left(\frac{\partial^2 u}{\partial x^2} + \frac{\partial^2 u}{\partial y^2} + \frac{\partial^2 u}{\partial z^2}\right) + \mathrm{s}_u \tag{2.9}$$

Y direction:

$$\rho\left(\frac{\partial v}{\partial t} + u\frac{\partial v}{\partial x} + v\frac{\partial v}{\partial y} + w\frac{\partial v}{\partial z}\right) = -\frac{\partial p}{\partial y} + \mu\left(\frac{\partial^2 v}{\partial x^2} + \frac{\partial^2 v}{\partial y^2} + \frac{\partial^2 v}{\partial z^2}\right) + s_v \tag{2.10}$$

Z direction:

$$\rho\left(\frac{\partial w}{\partial t}+u\frac{\partial w}{\partial x}+v\frac{\partial w}{\partial y}+w\frac{\partial w}{\partial z}\right)=-\frac{\partial p}{\partial z}+\mu\left(\frac{\partial^2 w}{\partial x^2}+\frac{\partial^2 w}{\partial y^2}+\frac{\partial^2 w}{\partial z^2}\right)+s_w \quad (2.11)$$

The continuity equation for incompressible fluid in Cartesian coordinate system can also be expressed as:

$$\frac{\partial u}{\partial x}+\frac{\partial v}{\partial y}+\frac{\partial w}{\partial z}=0 \quad (2.12)$$

Unlike algebraic equations, the Navier-Stokes equations are differential equations that do not explicitly establish relationships among the variables of interest (e.g. pressure and velocity). Rather they establish relationships among the rates of change.

The three momentum equations combined with the continuity equation provide a complete mathematical description of the flow of an incompressible Newtonian fluid. The Navier-Stokes equations provide four equations and where there are four unknown (u, v, w and p). This implies that the problem can be solved by manipulating simultaneous solution of the equations. However, they are not amenable to exact mathematical solution except in a few cases because they are non-linear, second order partial differential equations.

In order to solve the Navier-Stokes equations the partial differential equations should be replaced by a set of algebraic equations. To do this their numerical analogue must be generated by a process called discretization. There are various techniques of numerical discretization:

A) Finite element
B) Finite difference
C) Finite volume
D) Spectral methods.

For this study only the finite difference and finite volume methods will be discussed in detail.

2.3 The Finite Difference Method

The finite difference method (FDM) is the oldest method for numerical solution of partial differential equations, which is believed to have been introduced by Euler in the 18th century.

In the FDM the solution domain is covered with a grid as shown in Figure 2-1 as an illustrative one-dimensional example. At each grid point, the differential equation is approximated by replacing the partial derivatives by approximations in terms of the nodal values of the function. The result is one algebraic equation per grid node in which the variable value at that and a certain number of neighbor nodes appear as unknowns.

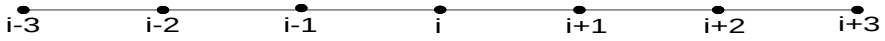

Figure 2-1: 1D Cartesian grid for FD method

Taylor series expansion is used to write the derivative of the variables at various points in space or time. As an example consider the discretization of dependent variable velocity *u* with respect to independent variable spatial coordinate *x*. Consider the curve in Figure 2-2 which represents the variation of *u* with respect to *x*, i.e., *u*(*x*).

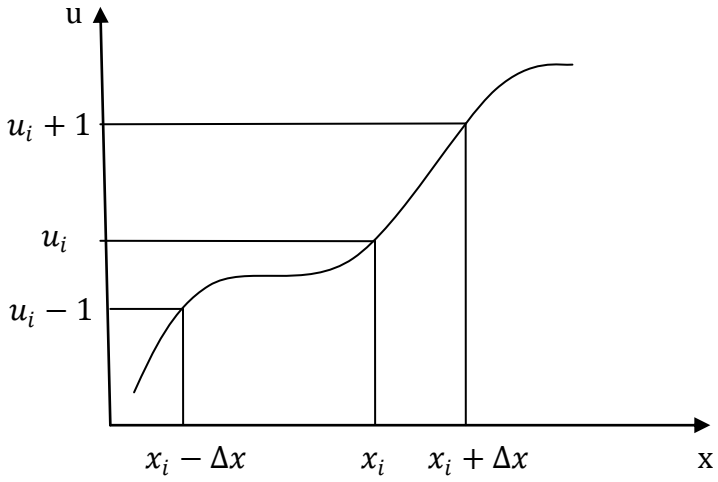

Figure 2-2: Points for Taylor series expansion

A set of discrete points, u_i's represent the curve *u*(*x*) after discretization. Taylor series expansion can be used to relate each discretized point. Thus the velocity u_i can be expressed in terms of Taylor series expansion about point *i* as:

$$u_{i+1=}\, u_i \; + \left(\frac{\partial u}{\partial x}\right)\Delta x + \left(\frac{\partial^2 u}{\partial x^2}\right)\frac{(\Delta x)^2}{2} + \left(\frac{\partial^3 u}{\partial x^3}\right)\frac{(\Delta x)^3}{6} + \cdots \tag{2.13}$$

$$u_{i-1=}\, u_i \; - \left(\frac{\partial u}{\partial x}\right)\Delta x + \left(\frac{\partial^2 u}{\partial x^2}\right)\frac{(\Delta x)^2}{2} - \left(\frac{\partial^3 u}{\partial x^3}\right)\frac{(\Delta x)^3}{6} + \cdots \tag{2.14}$$

The mathematical solution will be exact, if Δx is small and the number of terms are infinite. Ignoring terms leads to an error called truncation error. For the second order expression, the truncation error is:

$$\sum_{n=3}^{\infty} \left(\frac{\partial^n u}{\partial x^n}\right) \frac{(\Delta x)^{n-1}}{n!} \tag{2.15}$$

By subtracting or adding Equations (2.13) and (2.14), a new equation can be found for the first and second derivatives at central position *i*. These derivatives are:

$$\left(\frac{\partial u}{\partial x}\right)_i = \frac{u_{i+1} - u_{i-1}}{2\Delta x} - \left(\frac{\partial^3 u}{\partial x^3}\right) \frac{(\Delta x)^2}{6} \tag{2.16}$$

$$\left(\frac{\partial^2 u}{\partial x^2}\right)_i = \frac{u_{i+1} - 2u_i + u_{i+1}}{2\Delta x} + O(\Delta x^2) \tag{2.17}$$

Equations (2.16) and (2.17) are known as central difference equations to the first and second derivative, respectively. Alternatively, these can be found in a separate manner by considering Equations (2.13) or (2.14) in isolation. Looking at Equation (2.13), the first derivative can be formed as:

$$\left(\frac{\partial u}{\partial x}\right)_i = \frac{u_{i+1} - u_{i-1}}{\Delta x} - \left(\frac{\partial^2 u}{\partial x^2}\right) \frac{\Delta x}{2} \tag{2.18}$$

This is known as a forward difference approximation. Similarly, another first order derivative can be formed by considering Equation (2.14):

$$\left(\frac{\partial u}{\partial x}\right)_i = \frac{u_{i} - u_{i-1}}{\Delta x} - \left(\frac{\partial^2 u}{\partial x^2}\right) \frac{\Delta x}{2} \tag{2.19}$$

This is known as a backward difference approximation. Considering the above expressions, the different formulas are classified by either considering the geometrical relationship of points (central, backward and forward difference) or by the accuracy of the expression (for instance central difference is second order accurate as higher terms are neglected).

It is also possible to obtain higher order approximations by applying Taylor series expansion for different numbers of points. For instance, if a 3 point cluster is considered it would result in a second order approximation for the forward difference (Equation 2.20) and backward difference (Equation 2.21), rather than a first order approximation.

$$\left(\frac{\partial u}{\partial x}\right)_i = \frac{1}{2\Delta x} \left(-3u_i + 4u_{i+1} + u_{i+2}\right) + O(\Delta x)^2 \tag{2.20}$$

$$\left(\frac{\partial u}{\partial x}\right)_i = \frac{1}{2\Delta x} \left(u_{i-2} - 4u_{i-1} + 3u_i\right) + O(\Delta x)^2 \tag{2.21}$$

Using the above expressions a numerical analogue of the partial differential can be created. In order to apply FDM of discretization to the whole flow field:

1. Many points (nodes) are placed in the domain to be simulated.

2. The derivatives of the flow variables are written in the difference form at each of these points by relating the values of the variables at each point to its neighboring points.
3. The above process is applied at all points in the domain, a set of equations are obtained which are solved numerically to give the values of the variables (pressure and velocity).

Even though FDM is the easiest method to use for simple geometries it has the following limitations:

1. Conservation (mass, momentum, energy etc) is not enforced unless special care is taken.
2. It is used for simple geometries and cannot be used for complex geometries.

Because of these limitations, FDM is not used in CFD codes. Rather a finite volume method which overcomes these limitations is used in most of the CFD codes.

2.4 The Finite Volume Method

The finite volume method (FVM) uses the integral form of the conservation equations as its starting point. The solution domain is subdivided into a finite number of contiguous control volumes (CVs) as shown in Figure 2-3 and the conservation equations are applied to each CV. The values of the variables are calculated in computational nodes which are located at the centroid of each CV. Interpolation is used to express variable values at the CV surface in terms of the nodal (CV-center) values. Appropriate quadrature formulae are used to approximate surface and volume integrals. As a result, one obtains an algebraic equation for each CV, in which a number of nodal values appear.

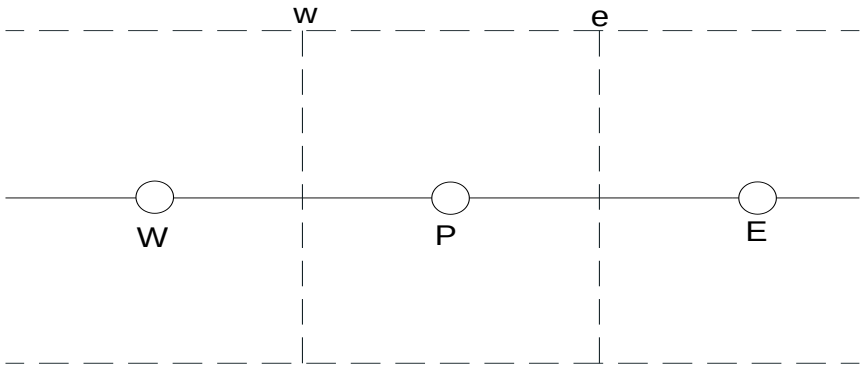

Figure 2-3: Finite volume in one dimension

Consider a finite volume or cell shown in Figure 2-3. The partial differential equation is discretized about a reference point *P* (centroid of the control volume). The neighboring

volumes are denoted as *W*, volume to the west side of *P*, and *E*, volume to the east side of *P*. *w* and *e* are the boundary faces of the volume with centroid *P*. The second derivative of the variable at *P* can be written as:

$$\left(\frac{\partial^2 u}{\partial x^2}\right) = \frac{[(\frac{\partial u}{\partial x})_e - (\frac{\partial u}{\partial x})_w]}{x_e - x_w} \tag{2.22}$$

The first derivative at volume faces can be written as to be the difference in the value of the variables at the neighboring volume centroids:

$$[\frac{\partial u}{\partial x}]_e = \frac{u_{E-u_P}}{x_{E-x_p}} \tag{2.23}$$

$$[\frac{\partial u}{\partial x}]_w = \frac{u_{P-u_W}}{x_{P-x_W}} \tag{2.24}$$

The finite volume method has the following advantages:

A) The most compelling feature of the FVM is that the resulting solution satisfies the conservation of quantities such as mass, momentum, and energy. This is exactly satisfied for any control volume as well as for the whole computational domain and for any number of control volumes.
B) The finite volume method can accommodate any type of grid, so it is suitable for complex geometries.
C) The finite volume method is simple to understand and program.

2.5 Solution Algorithm for Navier-Stokes Equation in Steady Flow

2.5.1 Introduction

The momentum and continuity equations for 2D steady (the velocity doesn't change with respect to time) and incompressible (density of the fluid doesn't change with respect to time) flow is given by:

X-momentum equation:

$$\frac{\partial}{\partial x}(\rho uu) + \frac{\partial}{\partial y}(\rho vu) = \frac{\partial}{\partial x}\left(\mu\frac{\partial u}{\partial x}\right) + \frac{\partial}{\partial y}\left(\mu\frac{\partial u}{\partial y}\right) - \frac{\partial p}{\partial x} + S_u \tag{2.25}$$

Y-momentum equation:

$$\frac{\partial}{\partial x}(\rho uv) + \frac{\partial}{\partial y}(\rho vv) = \frac{\partial}{\partial x}\left(\mu\frac{\partial v}{\partial x}\right) + \frac{\partial}{\partial y}\left(\mu\frac{\partial v}{\partial y}\right) - \frac{\partial p}{\partial y} + S_v \tag{2.26}$$

Continuity equation:

$$\frac{\partial}{\partial x}(\rho u) + \frac{\partial}{\partial y}(\rho v) = 0 \tag{2.27}$$

The solution of Equations (2.25)-(2.27) presents two problems:

- The momentum equation contains non-linear quantities. For example, the first term of Equation (2.25) is the x-derivative of ρu^2.
- All three equations are intricately coupled because every velocity component appears in each momentum equation and in the continuity equation.

To solve the above equations, an iterative solution strategy is employed. There are several different methods:

A) Semi-Implicit Method for Pressure Linked Equations (SIMPLE)
B) SIMPLE Revised (SIMPLER)
C) SIMPLE-Consistent (SIMPLEC)
D) Pressure Implicit with Splitting of Operators (PISO)

This study only considers the SIMPLE algorithm in detail for two reasons. First, it is relatively straightforward and has been successfully implemented in numerous CFD procedures. Second, it can produce savings in computational effort due to improved convergence.

2.5.2 Types of Grids

The finite volume method starts with the discretization of the flow domain and the Navier-Stokes equation. Depending on where the flow variables (velocity and pressure) are located, there are two types of grids. These are:

A) Collocated Grid Arrangement
B) Staggered Grid Arrangement

Collocated Grid Arrangement

In collocated grid arrangement the velocities are defined at the same location as the scalar variables such as pressure, temperature, etc. This arrangement seems logical. However, if velocities and pressures are both defined at the nodes of an ordinary control volume a highly non- uniform pressure field can act like a uniform field in the discretized equations. To demonstrate this, consider the two dimensional situation shown in Figure 2-4 where a uniform grid is used for simplicity.

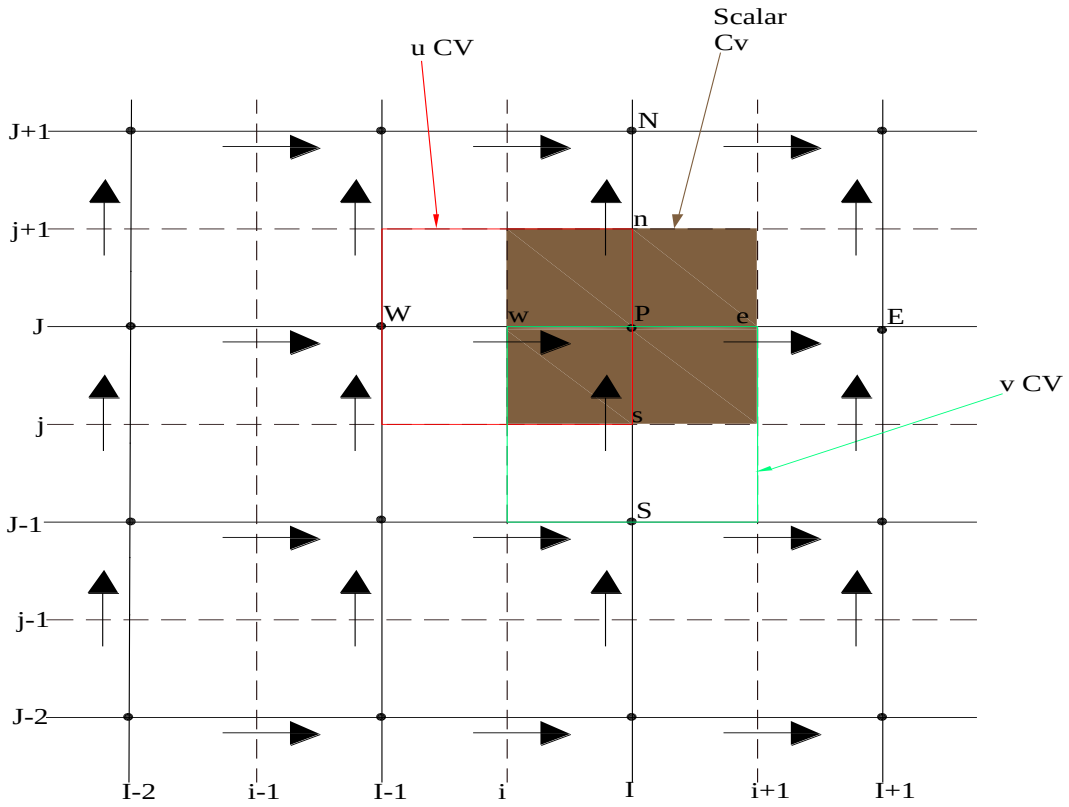

Figure 2-4: Checker-board pressure field

If pressures at *e* and *w* are obtained by linear interpolation, the pressure gradient term $\partial p/\partial x$ in the x-momentum equation is given by

$$\frac{\partial p}{\partial x} = \frac{p_e - p_w}{\delta x} = \frac{\left(\frac{p_E + p_P}{2}\right) - \left(\frac{p_P + p_w}{2}\right)}{\delta x} = \frac{p_E - p_W}{2\delta x} = \frac{100 - 100}{2\delta x} = 0$$

Similarly, the pressure gradient $\partial p/\partial y$ for the y-momentum equation is:

$$\frac{\partial p}{\partial y} = \frac{p_n - p_s}{\delta y} = \frac{\left(\frac{p_N + p_P}{2}\right) - \left(\frac{p_P - p_S}{2}\right)}{\delta y} = \frac{p_N - p_S}{2\delta y} = \frac{100 - 100}{2\delta y} = 0$$

As it is seen in the above expressions the pressure at the nodal point *P* is zero which is unrealistic and non-physical. It is clear that, if the velocities are defined at the scalar grid nodes, the influence of pressure is not properly represented in the discretized momentum equations.

Staggered Grid Arrangement

A remedy to solve the problem associated with collocated grid arrangement is to use a staggered grid for velocity components. The idea is to evaluate scalar variables, such as pressure, density, temperature etc., at ordinary nodal points but to calculate velocity components on staggered grids centered around the cell faces. Consider the use of a staggered grid arrangement as shown in Figure 2-5. The scalar variables, including pressure, are stored at the nodes marked (●). The velocities are defined at the (scalar) cell faces in between the nodes and are indicated by arrows.

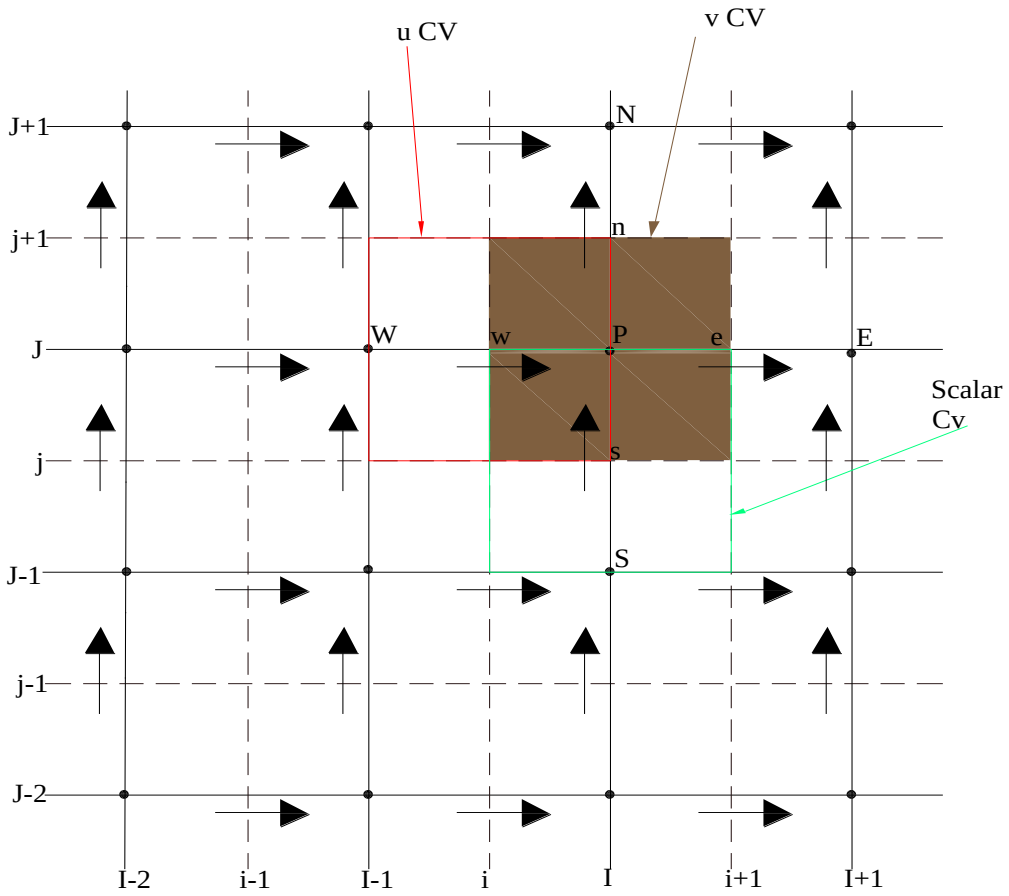

Figure 2-5: 2D staggered grid arrangement

Horizontal (→) arrows indicate the locations for the *u*-velocities and vertical (↑) arrows denote those for the *v*-velocities. *u*-velocities are stored at scalar cell faces *e* and *w* and the *v*-velocities at faces *n* and *s*.

In staggered grid arrangement the pressure gradients are evaluated at a location where the velocities are located i.e. at CV boundary points.

Consider the checker board pressure field shown in Figure 2-6. The pressure gradient term $\partial p/\partial x$ is given by:

$$\left.\frac{\partial p}{\partial x}\right|_w = \frac{p_p - p_W}{\Delta x_u} = \frac{50-100}{\Delta x_u} \neq 0 \tag{2.28}$$

Similarly, $\partial p/\partial y$ for the y-control volume is given by:

$$\left.\frac{\partial p}{\partial y}\right|_s = \frac{p_p - p_s}{\Delta y_v} = \frac{50-100}{\Delta y_v} \neq 0 \tag{2.29}$$

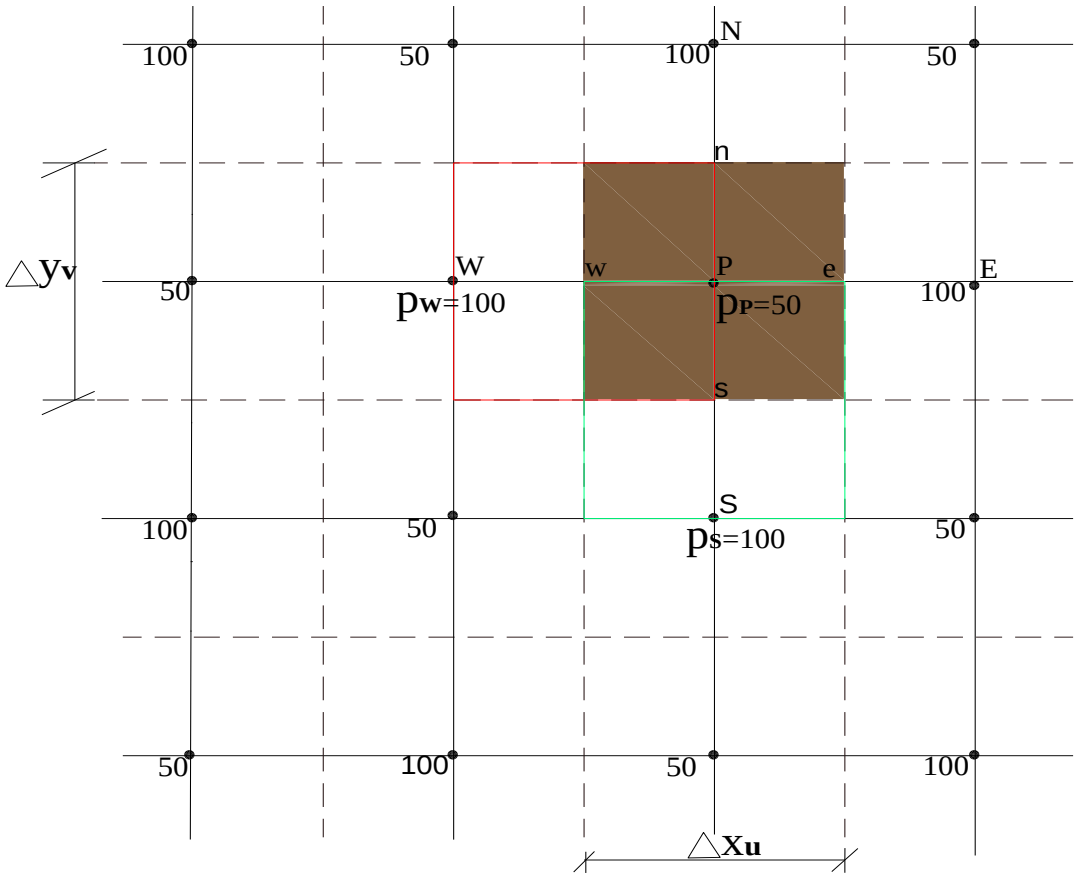

Figure 2-6: Checker board of pressure field

Substituting the values of pressures (as shown in Figure 2-6) into Equations 2.28 and 2.29 yields non-zero pressure gradient terms. The staggering of the velocity avoids the unrealistic behavior of the discretized momentum equation for spatially oscillating pressures like the 'checker-board' field. A further advantage of staggered grid arrangement is that it is computationally efficient in such a way that it has low memory requirement.

2.5.3 Discretization of Momentum Equations

Before discussing the discretization of the momentum equations, first the numbering of the staggered grid arrangement must be explored. Consider the staggered grid arrangement as shown in Figure 2-7.

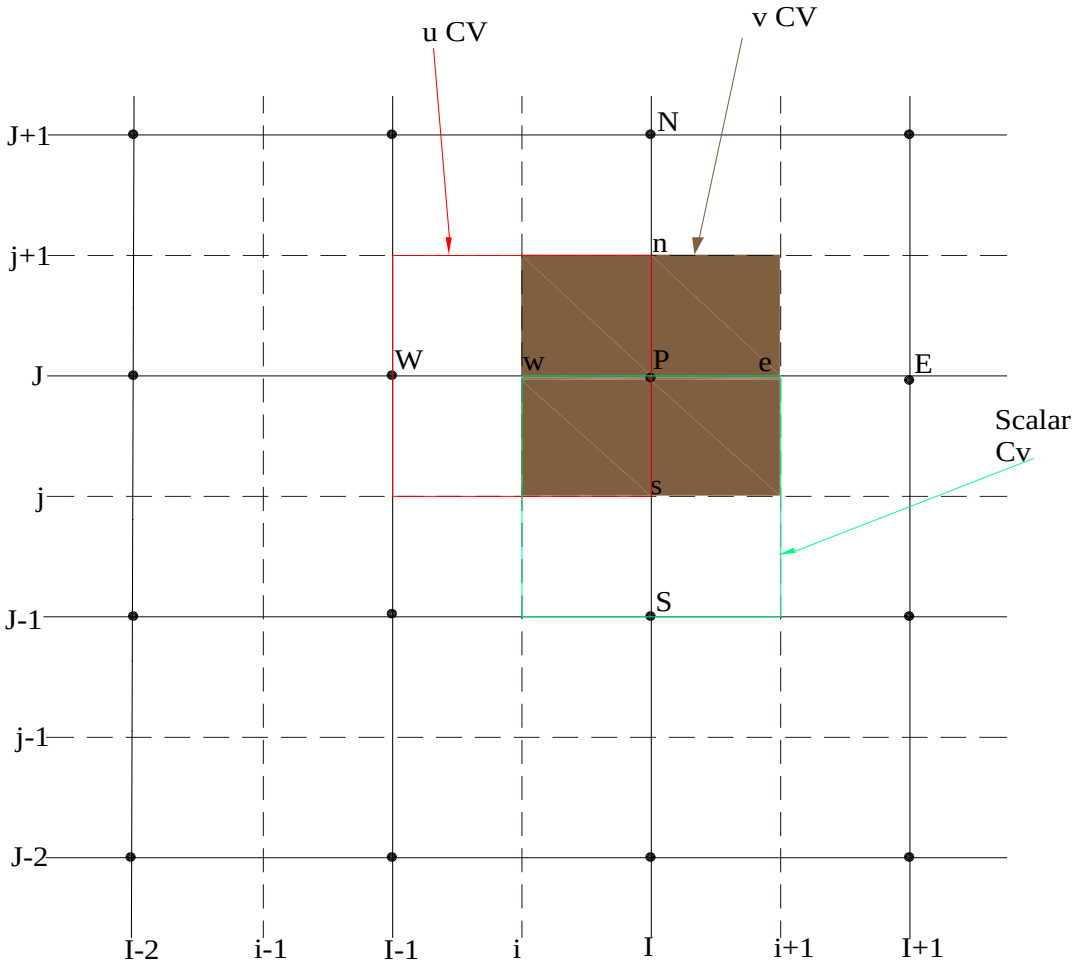

Figure 2-7: Staggered grid arrangements

In Figure 2-7 the unbroken grid lines are numbered using capital letters. In the x-direction the numbering is I-1, I, I+1, etc. and in the y-direction J-1, J, J+1, etc. The dashed lines that construct the cell faces are denoted by lower case letters i-1, i, i+1 and j-1, j, j+1 in the x-and y-directions, respectively.

A subscript system based on this numbering allows the locations of grid nodes and cell faces to be defined with precision. Scalar nodes, located at the intersection of two grid lines, are identified by two capital letters: e.g., point *P* in Figure 2-7 is denoted by (I, J).

The *u*-velocities are stored at the *e*- and *w*-cell faces of a scalar control volume. These are located at the intersection of a line defining a cell boundary and a grid line and are, therefore, defined by a combination of a lower case letter and a capital letter, e.g., the *w*-face of the cell point *P* is identified by (i, J). For the same reasons the storage locations for the *v*-velocities are combinations of a capital and a lower case letter: e.g., the *s*-face is given by (I, j).

Discretization of the x-momentum equation

Figure 2-8 shows a *u* control volume and neighboring velocity components which is used for the discretzation of the *x*-momentum equation.

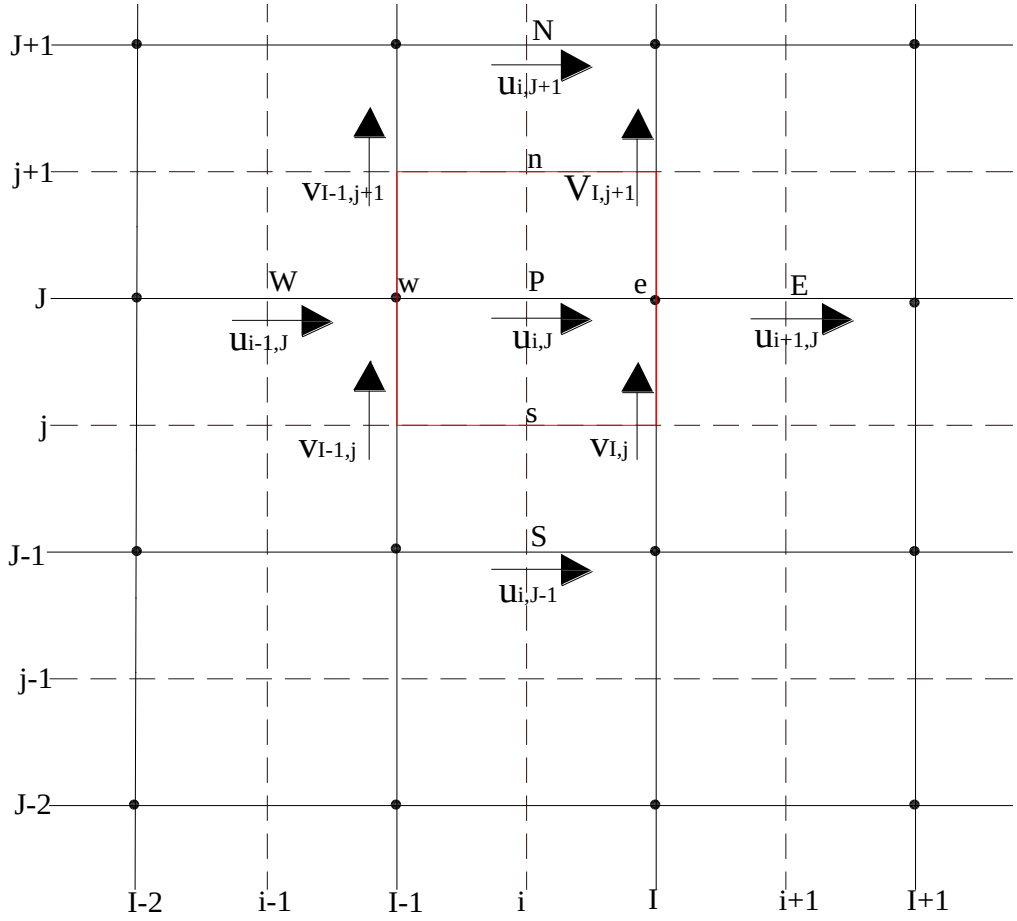

Figure 2-8: *u*-control volume and its neighboring velocity components

Integrating the *x*-momentum equation given by Equation (2.25) over the control volume shown in figure 2-8:

$$\int_{CV} \frac{d}{dx}(\rho uu)dV + \int_{CV} \frac{d}{dy}(\rho vu)dV$$

$$= \int_{CV} \frac{d}{dx}\left(\mu \frac{du}{dx}\right) dV + \int_{CV} \frac{d}{dy}(\mu \frac{du}{dy})dV + \int_{CV} -\frac{\partial p}{\partial x} dV + \int_{cv} s_u$$

Assuming constant area, constant viscosity and constant density the above integral yields:

$$(\rho uu)_e - (\rho uu)_w + (\rho vu)_n - (\rho vu)_s$$

$$= \mu \left(\frac{\partial u}{\partial x}\right)_e - \mu \left(\frac{\partial u}{\partial x}\right)_w + \mu \left(\frac{\partial u}{\partial y}\right)_n - \mu(\frac{\partial u}{\partial y})_s - \Delta V \frac{p_e - p_w}{\Delta x} + \Delta V s_u$$

Assume the convective fluxes are known:

$$F_n = (\rho v)_n \qquad F_s = (\rho v)_s$$

$$F_e = (\rho u)_e \qquad F_w = (\rho u)_w$$

A central difference scheme (CDS) is used for the viscous term and upwind difference scheme (UDS) is used for convective term:

$$F_e u_P - F_w u_W + \frac{F_n}{2}(u_N + u_P) - \frac{F_s}{2}(u_P + u_S)$$
$$= \left(\frac{\mu}{\Delta x}\right)(u_E - u_P) - \left(\frac{\mu}{\Delta x}\right)(u_P - u_W) + \frac{\mu}{\Delta y}(u_N - u_P) - \frac{\mu}{\Delta y}(u_P - u_S) - \Delta V \frac{p_e - p_w}{\Delta x} + \Delta V s_u$$

Rewriting the convective fluxes:

$$F_e = (\rho u)_e = \rho \frac{(u_{i,J} + u_{i+1,J})}{2} \qquad F_w = (\rho u)_w = \rho \frac{(u_{i-1,J} + u_{i,J})}{2}$$

$$F_n = (\rho v)_n = \rho \frac{(V_{I-1,j+1} + V_{I,j+1})}{2} \qquad F_s = (\rho v)_s = \rho \frac{(V_{I-1,j} + V_{I,j})}{2}$$

Substituting the convective fluxes and rearranging the terms:

$$a_{i,J} u_{i,J} = a_{i-1,J} u_{i-1,J} + a_{i+1,J} u_{i+1,J} + a_{i,J-1} u_{i,J-1} + \qquad (2.30)$$

$$a_{i,J+1} u_{i,J+1} + s_u \Delta V - \frac{p_{I,J} - p_{I-1,J}}{\Delta x} \Delta V$$

where:

$$a_{i,J} = F_e + \frac{1}{2}F_n - \frac{1}{2}F_s + D_e + D_w + D_n + D_s$$

$$a_{i-1,J} = F_w + D_w$$

$$a_{i+1,J} = D_e$$

$a_{i,J-1} = \frac{1}{2}F_s + D_s$

$a_{i,J+1} = -\frac{1}{2}F_n + D_n$

$D_e = \frac{\mu}{\Delta x}$ $\quad D_w = \frac{\mu}{\Delta x}$ $\quad D_n = \frac{\mu}{\Delta y}$ $\quad D_s = \frac{\mu}{\Delta y}$

Equation (2.30) can be re-written as:

$$a_{i,J}u_{i,J} = \sum_{nb} a_{nb}u_{nb} + b_{i,J} - (p_{I,J} - p_{I-1,J})A_{i,J} \quad (2.31)$$

Where:

$a_{nb}u_{nb} = a_{i-1,J}u_{i-1,J} + a_{i+1,J}u_{i+1,J} + a_{i,J-1}u_{i,J-1} + a_{i,J+1}u_{i,J+1}$

$b_{i,J} = s_u \Delta V$ $\quad A_{i,J} = \Delta V / \Delta x$

Discretization of the y-momentum equation

Figure 2-9 shows a *v* control volume and neighboring velocity components which is used for the discretzation of the *y*-momentum equation.

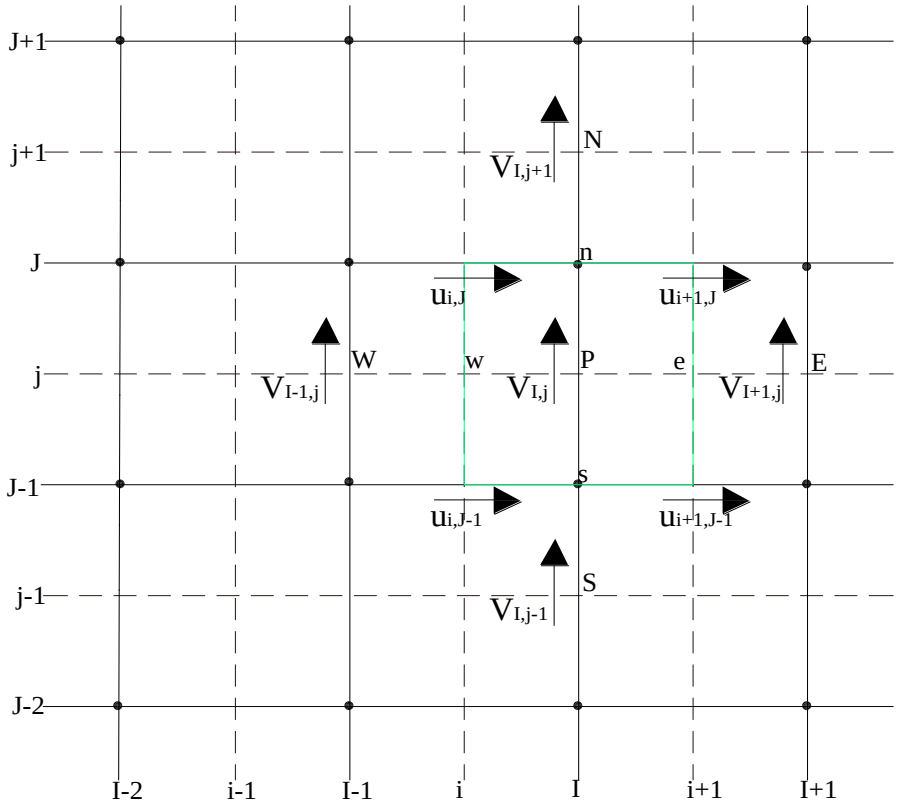

Figure 2-9: *v*-control volume and its neighboring velocity components

Similarly, integrating the momentum equation (Equation 2.26) in the *y*-direction over the control volume and rearranging all the terms:

$$a_{I,j}v_{I,j} = a_{I,j-1}v_{I,j-1} + a_{I+1,j}v_{I+1,j} + a_{I,j+1}v_{I,j+1} + a_{I-1,j}v_{I-1,j} + s_u\Delta V - \frac{p_{I,J}-p_{I,J-1}}{\Delta y}\Delta V \quad (2.32)$$

where:

$$a_{I,j} = F_n + \frac{1}{2}F_e - \frac{1}{2}F_w + D_e + D_w + D_n + D_s$$

$$a_{I,j-1} = F_s + D_s \qquad a_{I,j+1} = D_n$$

$$a_{I+1,j} = -\frac{1}{2}F_e + D_e \qquad a_{I-1,j} = \frac{1}{2}F_w + D_w$$

$$F_e = (\rho u)_e = \rho\frac{(u_{i+1,J-1} + u_{i+1,J})}{2} \qquad F_n = (\rho v)_n = \rho\frac{(V_{I,j} + V_{I,j+1})}{2}$$

$$F_w = (\rho u)_w = \rho\frac{(u_{i,J} + u_{i,J-1})}{2} \qquad F_s = (\rho v)_s = \rho\frac{(V_{I,j} + V_{I,j-1})}{2}$$

$$D_e = \frac{\mu}{\Delta x} \qquad D_w = \frac{\mu}{\Delta x}$$

$$D_n = \frac{\mu}{\Delta y} \qquad D_s = \frac{\mu}{\Delta y}$$

Equation 2.32 can be rewritten as:

$$a_{I,j}v_{I,j} = \sum_{nb} a_{nb}v_{nb} + b_{I,j} - (p_{I,J} - p_{I,J-1})A_{I,j} \quad (2.33)$$

where:

$$a_{nb}v_{nb} = a_{I,j-1}v_{I,j-1} + a_{I+1,j}v_{I+1,j} + a_{I,j+1}v_{I,j+1} + a_{I-1,j}v_{I-1,j}$$

$$b_{I,j} = s_u\Delta V$$

$$A_{I,j} = \Delta V/\Delta y$$

2.5.4 The SIMPLE Algorithm

The acronym SIMPLE stands for Semi-Implicit Method for Pressure Linked Equations. It is a guess-and-correct (iterative), procedure for the calculation of pressure on the staggered grid arrangement. The SIMPLE algorithm is briefly outlined in Figure 2-10.

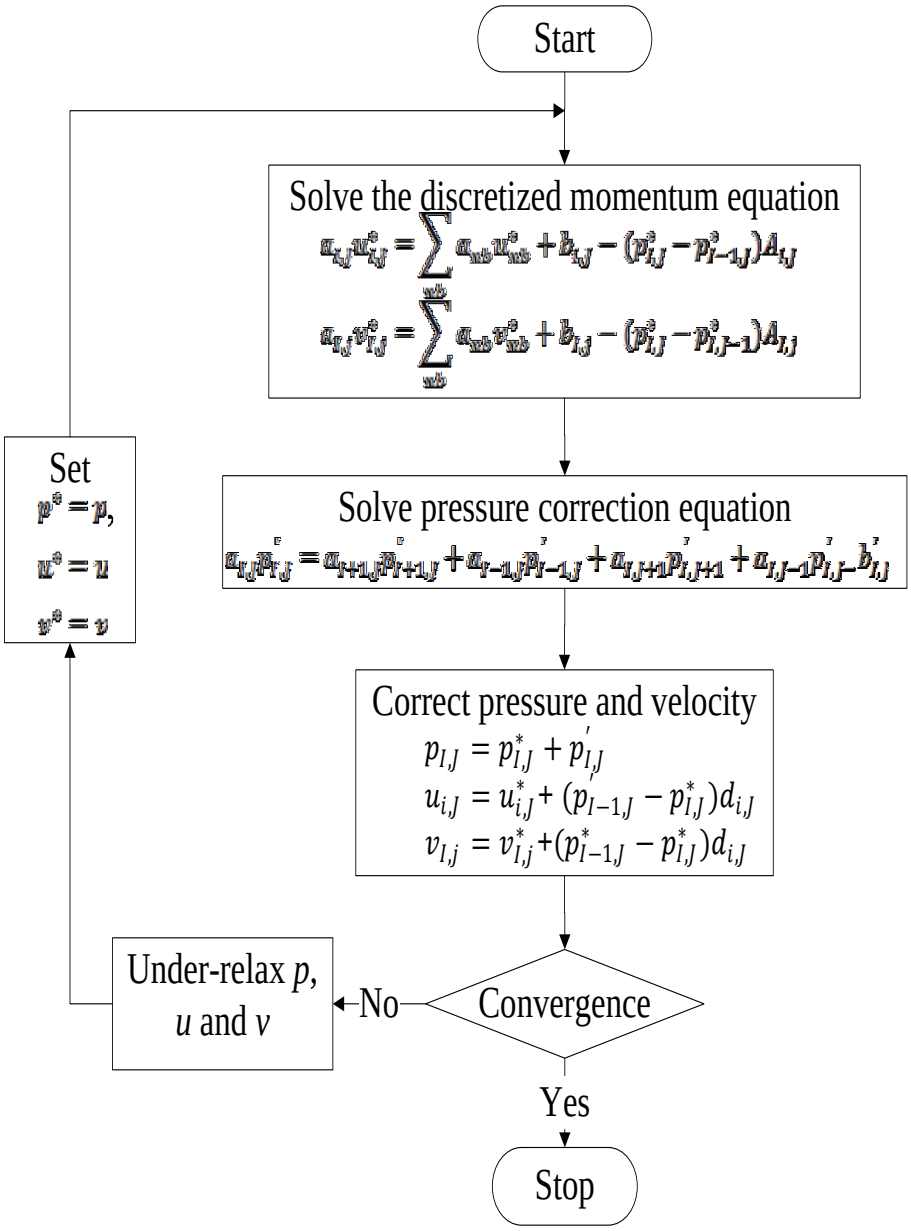

Figure 2-10: Flow chart for SIMPLE algorithm in steady flow

The calculations in the SIMPLE algorithm start by initially guessing pressure p^*. The discretized momentum equations given in Equation 2.31 and 2.33 are solved to give velocity components, u^* *and* v^* as follows:

$$a_{i,J}u^*_{i,J} = \sum_{nb} a_{nb}u^*_{nb} + b_{i,J} - (p^*_{I,J} - p^*_{I-1,J})A_{i,J} \quad (2.34)$$

$$a_{I,j}v^*_{I,j} = \sum_{nb} a_{nb}v^*_{nb} + b_{I,j} - (p^*_{I,J} - p^*_{I,J-1})A_{I,j} \quad (2.35)$$

Calculating $u^* \; and \; v^*$ and having p^* from initial guess, a correction is applied before proceeding to the next iteration. The new pressure *p* and the new velocities *u* and *v* after a correction is applied are given by:

$$p = p^* + p' \tag{2.36}$$

$$u = u^* + u' \tag{2.37}$$

$$v = v^* + v' \tag{2.38}$$

where p', $u' \; and \; v'$ are corrections for pressure and velocities, respectively.

The momentum equations can be re-written using the corrected pressure *p* and velocities u and v as:

$$a_{i,J} u_{i,J} = \sum_{nb} a_{nb} u_{nb} + b_{i,J} - (p_{I,J} - p_{I-1,J}) A_{i,J} \tag{2.39}$$

$$a_{I,j} v_{I,j} = \sum_{nb} a_{nb} v_{nb} + b_{I,j} - (p_{I,J} - p_{I,J-1}) A_{I,j} \tag{2.40}$$

Subtracting Equation (2.39) from (2.34) yields:

$$a_{i,J}\left(u_{i,J} - u^*_{i,J}\right) = \sum_{nb} a_{nb} \left(u_{nb} - u^*_{nb}\right) + \left(\left(p_{I-1,J} - p^*_{I-1,J}\right) - \left(p_{I,J} - p^*_{I,J}\right)\right) A_{i,J} \tag{2.41}$$

Rearranging Equations (2.36) and (2.37) and substituting into equation (2.44) gives:

$$a_{i,J} u'_{i,J} = \sum_{nb} a_{nb} u'_{nb} + (p'_{I-1,J} - p^*_{I,J}) A_{i,J} \tag{2.42}$$

Similarly, subtracting Equations (2.35) from (2.40) and equating Equations (2.36) and (2.38) results in:

$$a_{I,j} v'_{I,j} = \sum_{nb} a_{nb} v'_{nb} + (p^*_{I-1,J} - p^*_{I,J}) A_{i,J} \tag{2.43}$$

To simplify Equations (2.42) and (2.43), $\sum_{nb} a_{nb} u'_{nb}$ and $\sum_{nb} a_{nb} v'_{nb}$ terms are dropped. Leaving out these terms is the main approximation of the SIMPLE algorithm. The equations then simplify to:

$$u'_{i,J} = (p'_{I-1,J} - p^*_{I,J}) d_{i,J} \tag{2.44}$$

$$v'_{I,j} = (p^*_{I-1,J} - p^*_{I,J}) d_{I,j} \tag{2.45}$$

where:

$$d_{i,J} = \frac{A_{i,J}}{a_{i,J}} \qquad\qquad d_{I,j} = \frac{A_{I,j}}{a_{I,j}}$$

Substituting Equations (2.44) and (2.45) into Equations (2.37) and (2.38), respectively, yields:

$$u_{i,J} = u^*_{i,J} + (p'_{I-1,J} - p^*_{I,J})d_{i,J} \quad (2.46)$$

$$v_{I,j} = v^*_{I,j} + (p^*_{I-1,J} - p^*_{I,J})d_{i,J} \quad (2.47)$$

Up to now, only the momentum equations have been considered but the velocity fields should also satisfy the continuity equation. Integrating the continuity equation (Equation 2.27) over the scalar control volume shown in Figure 2-11:

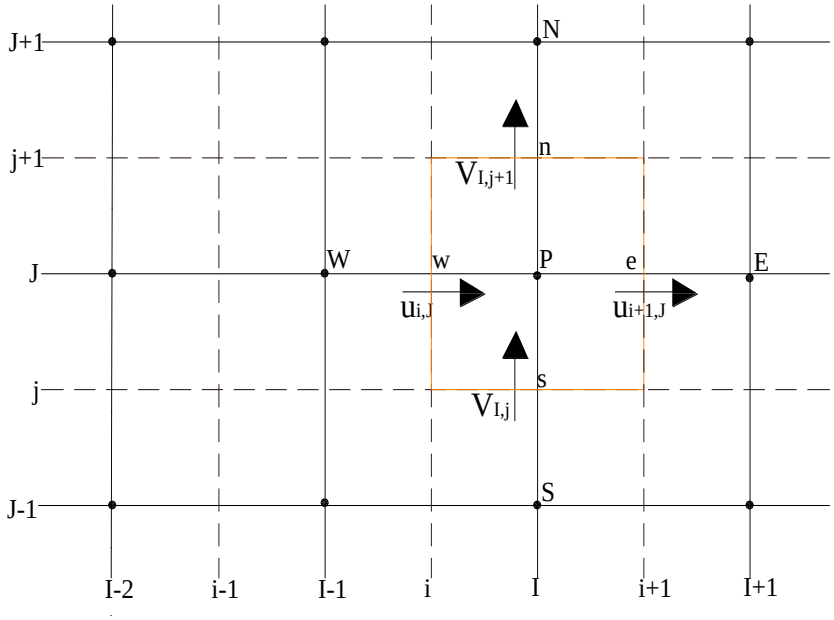

Figure 2-11: Scalar control volume for the discretization of the continuity equation

$$\left[(\rho uA)_{i+1,J} - (\rho uA)_{i,J}\right] + \left[(\rho vA)_{I,j+1} - (\rho vA)_{I,j}\right] = 0 \quad (2.48)$$

Substitution of the corrected velocities of Equations (2.46) and (2.47) into the discretized continuity Equation (2.48) and rearranging all terms gives:

$$a_{I,J}p'_{I,J} = a_{I+1,J}p'_{I+1,J} + a_{I-1,J}p'_{I-1,J} + a_{I,J+1}p'_{I,J+1} + a_{I,J-1}p'_{I,J} - b'_{I,J} \quad (2.49)$$

where:

$$a_{I,J} = a_{I+1,J} + a_{I-1,J} + a_{I,J+1} + a_{I,J-1}$$

$$a_{I+1,J} = (\rho dA)_{i+1,J}$$

$$a_{I-1,J} = (\rho dA)_{i,J}$$

$$a_{I,J+1} = (\rho dA)_{I,j+1}$$

$$a_{I,J-1} = (\rho dA)_{I,j}$$

$$b'_{I,J} = (\rho u^* A)_{i,J} - (\rho u^* A)_{i+1,J} + (\rho v^* A)_{I,j} - (\rho v^* A)_{I,J+1}$$

Equation (2.49) represents the discretized continuity equation which is used to apply the pressure correction p'.

2.5.5 Under-Relaxation

When applying the pressure correction it may cause divergence. To avoid this, only a fraction of the pressure correction is used or under-relaxation is applied.

Under-relaxation is used for the pressure correction equation during the iterative process to yield a new and improved pressure p^{new} because it is susceptible to divergence. The new pressure p^{new} is given by:

$$p^{new} = p^* + \alpha_p p' \tag{2.50}$$

where α_p is the pressure under-relaxation factor. α_p is taken between 0 and 1. A correct choice of under-relaxation factor α is essential for cost-effective simulations. Too large of a value of α may lead to oscillatory or even divergent iterative solutions, and a value which is too small will cause extremely slow convergence.

The velocities are also under-relaxed. The iteratively improved velocity components u^{new} and v^{new} are obtained from

$$u^{new} = \alpha_u u + (1 - \alpha_u) u^{n-1} \tag{2.51}$$

$$v^{new} = \alpha_v v + (1 - \alpha_v) v^{n-1} \tag{2.52}$$

where α_u and α_v are the *u*-and *v*-velocity under-relaxation factors, *u* and *v* are the corrected velocity components without relaxation, and u^{n-1} and v^{n-1} represents their values obtained in the previous iteration.

2.6 Solution Algorithm for Navier-Stokes Equation in Unsteady Flow

Unsteady flow involves the change in velocity with respect to time. The momentum equation for 2D unsteady flow is given by:

x–direction:

$$\rho\left(\frac{\partial u}{\partial t} + u\frac{\partial u}{\partial x} + v\frac{\partial u}{\partial y} + w\frac{\partial u}{\partial z}\right) = -\frac{\partial p}{\partial x} + \mu\left(\frac{\partial^2 u}{\partial x^2} + \frac{\partial^2 u}{\partial y^2} + \frac{\partial^2 u}{\partial z^2}\right) + s_u \tag{2.53}$$

y–direction:

$$\rho\left(\frac{\partial v}{\partial t}+u\frac{\partial v}{\partial x}+v\frac{\partial v}{\partial y}+w\frac{\partial v}{\partial z}\right)=-\frac{\partial p}{\partial y}+\mu\left(\frac{\partial^2 v}{\partial x^2}+\frac{\partial^2 v}{\partial y^2}+\frac{\partial^2 v}{\partial z^2}\right)+S_v \quad (2.54)$$

An iterative solution strategy is also employed to solve the equations similar to the case of steady flow. In order to employ the solution technique, the *x* and *y* momentum equations are discretized over their respective control volume.

Discretization of the x-momentum equation

Integrating Equation 2.53 over the control volume shown in Figure 2-8 produces:

$$\int_{CV}\frac{d}{dt}(\rho u)dV+\int_{CV}\frac{d}{dx}(\rho uu)dV+\int_{CV}\frac{d}{dy}(\rho vu)dV$$

$$=\int_{CV}\frac{d}{dx}\left(\mu\frac{du}{dx}\right)dV+\int_{CV}\frac{d}{dy}\left(\mu\frac{du}{dy}\right)dV+\int_{CV}-\frac{\partial p}{\partial x}dV+\int_{\Delta V}s_u\,dV$$

Applying the fully implicit scheme, taking the values of pressure and velocity at the new time step, the above integral yields:

$$\frac{\rho(u-u_o)}{\Delta t}\Delta V+(\rho uu)_e-(\rho uu)_w+(\rho vu)_n-(\rho vu)_s=\mu\left(\frac{\partial u}{\partial x}\right)_e-\mu\left(\frac{\partial u}{\partial x}\right)_w+\mu\left(\frac{\partial u}{\partial y}\right)_n-\mu\left(\frac{\partial u}{\partial y}\right)_s-\Delta V\frac{p_e-p_w}{\Delta x}+\Delta V s_u$$

where u_o is the velocity at the old time step.

Assuming the convective fluxes are known:

$$F_e=(\rho u)_e \qquad F_w=(\rho u)_w$$

$$F_n=(\rho v)_n \qquad F_s=(\rho v)_s$$

Then, substituting the convective fluxes into the results of the integral yields:

$$\frac{\rho(u-u_o)}{\Delta t}\Delta V+F_e u_P-F_w u_W+\frac{F_n}{2}(u_N+u_P)-\frac{F_s}{2}(u_P+u_S)$$

$$=\left(\frac{\mu}{\Delta x}\right)(u_E-u_P)-\left(\frac{\mu}{\Delta x}\right)(u_P-u_W)+\frac{\mu}{\Delta y}(u_N-u_P)-\frac{\mu}{\Delta y}(u_P-u_S)-\Delta V\frac{p_e-p_w}{\Delta x}+\Delta V s_u$$

where the convective fluxes are given by:

$$F_e=(\rho u)_e=\rho\frac{(u_{i,J}+u_{i+1,J})}{2} \qquad F_n=(\rho v)_n=\rho\frac{(V_{I-1,j+1}+V_{I,j+1})}{2}$$

$$F_w=(\rho u)_w=\rho\frac{(u_{i-1,J}+u_{i,J})}{2} \qquad F_s=(\rho v)_s=\rho\frac{(V_{I-1,j}+V_{I,j})}{2}$$

Rearranging the terms of the discretized momentum equation in the x *d*irection yields:

$$\left(a_{i,J} + \frac{\rho \Delta V}{\Delta t}\right) u_{i,J} = a_{i-1,J} u_{i-1,J} + a_{i+1,J} u_{i+1,J} + a_{i,J-1} u_{i,J-1} + a_{i,J+1} u_{i,J+1} + \quad (2.55)$$

$$s_u \Delta V - \frac{p_{I,J} - p_{I-1,J}}{\Delta x} \Delta V + \frac{\rho \Delta V}{\Delta t} u_{i,J}^o$$

The expressions for the coefficients of Equation 2.55 are similar to Equation 2.30. Equation 2.55 can be rewritten as:

$$\tilde{a}_{i,J} u_{i,J} = \sum_{nb} a_{nb} u_{nb} + b_{i,J} - (p_{I,J} - p_{I-1,J}) A_{i,J} \quad (2.56)$$

where:

$$a_{nb} u_{nb} = a_{i-1,J} u_{i-1,J} + a_{i+1,J} u_{i+1,J} + a_{i,J-1} u_{i,J-1} + a_{i,J+1} u_{i,J+1}$$

$$\tilde{a}_{i,J} = a_{i,J} + \frac{\rho \Delta V}{\Delta t}$$

$$b_{i,J} = s_u \Delta V + \frac{\rho \Delta V}{\Delta t} u_{i,J}^o$$

$$A_{i,J} = \Delta V / \Delta x$$

Discretization of the y-momentum equation

Similarly, integrating Equation 2.54 over the control volume shown in Figure 2-9 and rearranging all the terms yields:

$$\left(a_{I,j} + \frac{\rho \Delta V}{\Delta t}\right) v_{I,j} = a_{I,j-1} v_{I,j-1} + a_{I+1,j} v_{I+1,j} + a_{I,j+1} v_{I,j+1} + a_{I-1,j} v_{I-1,j} \quad (2.57)$$

$$s_u \Delta V - \frac{p_{I,J} - p_{I,J-1}}{\Delta y} \Delta V + \frac{\rho \Delta V}{\Delta t} v_{i,J}^o$$

The expressions for the coefficients of Equation 2.57 are similar to Equation 2.32. Equation 2.57 can be rewritten as:

$$\tilde{a}_{I,j} v_{I,j} = \sum_{nb} a_{nb} v_{nb} + b_{I,j} - (p_{I,J} - p_{I,J-1}) A_{I,j} \quad (2.58)$$

where:

$$\tilde{a}_{I,j} = a_{I,j} + \frac{\rho \Delta V}{\Delta t} \qquad b_{I,j} = s_u \Delta V + \frac{\rho \Delta V}{\Delta t} v_{i,J}^o \qquad A_{I,j} = \Delta V / \Delta y$$

$$a_{nb} v_{nb} = a_{I,j-1} v_{I,j-1} + a_{I+1,j} v_{I+1,j} + a_{I,j+1} v_{I,j+1} + a_{I-1,j} v_{I-1,j}$$

Similar to the case of steady flow, the Navier-Stokes equation for unsteady flow can be solved using iterative techniques like SIMPLE, SIMPLEC, SIMPLER, and PISO. For the current study the SIMPLE algorithm is considered as shown in Figure 2-12.

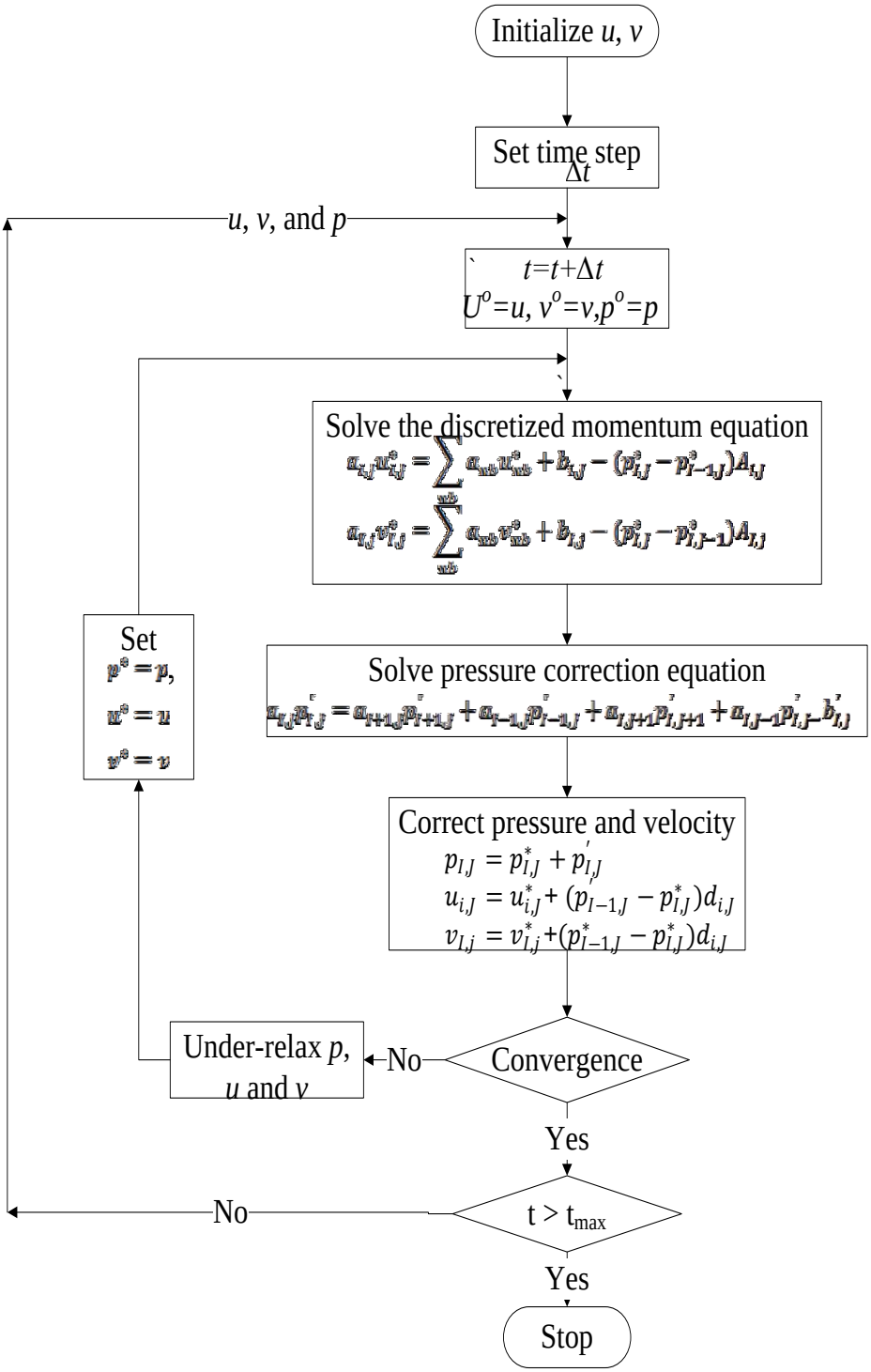

Figure 2-12: Flow chart for SIMPLE algorithm in unsteady flow

The SIMPLE algorithm for unsteady flow starts by initializing pressure and velocity at time t=0. The next step is to solve momentum and pressure correction equations until convergence is reached for each time step.

The velocity correction equations, which can be derived by following a similar procedure for the case of steady flow, are given by:

$$u_{i,J}^{'} = (p_{I-1,J}^{'} - p_{I,J}^{*})\hat{d}_{i,J} \tag{2.59}$$

$$v_{I,j}^{'} = (p_{I-1,J}^{*} - p_{I,J}^{*})\hat{d}_{I,j} \tag{2.60}$$

where:

$$\hat{d}_{i,J} = \frac{A_{i,J}}{\tilde{a}_{i,J}} \qquad\qquad \hat{d}_{I,j} = \frac{A_{I,j}}{\tilde{a}_{I,j}}$$

The corrected velocity is then given by:

$$u_{i,J} = u_{i,J}^{*} + (p_{I-1,J}^{'} - p_{I,J}^{*})\hat{d}_{i,J} \tag{2.61}$$

$$v_{I,j} = v_{I,j}^{*} + (p_{I-1,J}^{*} - p_{I,J}^{*})\hat{d}_{I,j} \tag{2.62}$$

The pressure correction equation is derived from the continuity equation. Even though incompressible flow is being considered, the same pressure correction equation that was used for steady flow is again applied, namely Equation 2.52.

2.7 Iterative Convergence and Residual

Flow problems, in general, require iteration like the case of SIMPLE algorithm. The final solution exactly satisfies the discretized flow equation in the interior of the domain and specified conditions on its boundaries. If the iteration sequence is convergent the difference between the final solution of the coupled set of discretized flow equations and the current solution after *k* iterations reduces as the number of iterations increases. Because of the limited computational effort and time the iteration sequence is truncated when the solution is close to the final solution, the truncation generates a contribution to the numerical errors.

To determine whether it is worth making additional effort to get closer to the final solution we would ideally like a truncation criterion in the form of single number that can be tested against a pre-set tolerance. There are different ways of constructing a practically useful truncation criterion in CFD, but by far the most common is based on residuals.

The discretization of the *x* and *y* momentum equation is given by Equation 2.31 and 2.33. The final values of the variable of interest (pressure and velocity) exactly satisfies these equations at all cells in the mesh but after a certain number of (*k* iterations) iterations there will be a difference between the left and the right hand side. The absolute value of this difference at mesh cell *i* is termed as the local residualR_i. The local residual for *x* and *y* momentum equation is given by:

$$(R_i^u)^{(k)} = \left|(a_{i,J}u_{i,J})_i^{(k)} - (\textstyle\sum_{nb} a_{nb}u_{nb})_i^{(k)} - (b_{i,J})_i^{(k)} + [(p_{I,J} - p_{I-1,J})A_{i,J}]_i^{(k)}\right| \tag{2.63}$$

$$(R_i^v)^{(k)} = \left|(a_{I,j}\, v_{I,j})_i^{(k)} - (\sum_{nb} a_{nb}\, v_{nb})_i^{(k)} - (b_{I,j})_i^{(k)} + [(p_{I,J} - p_{I,J-1})A_{i,J}]_i^{(k)}\right| \qquad (2.64)$$

where the superscript *k* indicates the current iteration count.

To determine the convergence behavior across the whole flow field, a global residual $\hat{R}$ is defined. Global residual $\hat{R}$ is simply the sum of local residual over all the control volume within the computational domain. After *k* iterations the global residual for the *x* and *y* momentum equation is given by:

$$(\hat{R}^u)^{(k)} = \sum_{i=1}^{M} (\hat{R}^u)^{(k)}$$

$$= \sum_{i=1}^{M} \left|(a_{i,J}\, u_{i,J})_i^{(k)} - (\sum_{nb} a_{nb}\, u_{nb})_i^{(k)} - (b_{i,J})_i^{(k)} + [(p_{I,J} - p_{I-1,J})A_{i,J}]_i^{(k)}\right| \qquad (2.65)$$

$$(\hat{R}^v)^{(k)} = \sum_{i=1}^{M} (\hat{R}^v)^{(k)}$$

$$= \sum_{i=1}^{M} \left|(a_{I,j}\, v_{I,j})_i^{(k)} - (\sum_{nb} a_{nb}\, v_{nb})_i^{(k)} - (b_{I,j})_i^{(k)} + [(p_{I,J} - p_{I,J-1})A_{i,J}]_i^{(k)}\right| \qquad (2.66)$$

The absolute value used in the expression of the local residual helps to prevent the cancellation of positive and negative values, which results in zero global residual while some or all of the local residuals are non-zero.

Observing Equations 2.65 and 2.66 the magnitude of the global residual $\hat{R}^u$ and $\hat{R}^v$ should decrease as we get to the final solution since the magnitude of the local residual also decreases in convergence sequence. As a result it might seem $\hat{R}^u$ and $\hat{R}^v$ be satisfactory numbers that indicate convergence, However that is not always the case. For instance the global residual will be larger in a simulation when the velocities have a large magnitude, for such a case we need to specify different truncation values for $\hat{R}^u$ and $\hat{R}^v$. To solve this problem we need to normalize the global residual $\hat{R}^u$ and $\hat{R}^v$ of the flow variables after *k* iterations as follows:

$$(\hat{R}^u{}_N)^{(k)} = \frac{(\hat{R}^u)^{(k)}}{\hat{F}_{Ru}} \qquad (2.67)$$

$$(\hat{R}^v{}_N)^{(k)} = \frac{(\hat{R}^v)^{(k)}}{\hat{F}_{Rv}} \qquad (2.68)$$

The normalization factor $\hat{F}_{Ru}$ and $\hat{F}_{Rv}$ are reference values of residual for flow variables *u* and *v*.

There are two common types of normalization techniques. The first method involves normalizing the global residual by its own size at k_o iteration, where $k_o \neq 1$ but usually 10. The normalized residual for the *x* and *y* momentum equations are given by:

$$\hat{F}_{Ru} = (\hat{R}^u)^{k_o} \qquad \Rightarrow \qquad (\hat{R}^u{}_N)^{(k)} = \frac{(\hat{R}^u)^{(k)}}{\hat{F}_{Ru}} \qquad (2.69)$$

$$\hat{F}_{Rv} = (\hat{R}^{v})^{k_o} \qquad \Rightarrow \qquad (\hat{R}^{v}{}_{N})^{(\mathrm{k})} = \frac{(\hat{R}^{v})^{(k)}}{\hat{F}_{Rv}} \tag{2.70}$$

The second method involves normalizing the global residual of the *x* and *y* momentum equations by the sum of the absolute value of the left hand side of Equation 2.31 and 2.33. The normalized residual for this method is then given by:

$$\hat{F}_{Ru} = \sum_{i=1}^{M} \left| (a_{i,J}\, u_{i,J})_i^{(k)} \right| \qquad \Rightarrow (\hat{R}^{u}{}_{N})^{(\mathrm{k})} = \frac{(\hat{R}^{u})^{(k)}}{\hat{F}_{Ru}} \tag{2.71}$$

$$\hat{F}_{Rv} = \sum_{i=1}^{M} \left| (a_{I,j}\, v_{I,j})_i^{(k)} \right| \qquad \Rightarrow (\hat{R}^{v}{}_{N})^{(\mathrm{k})} = \frac{(\hat{R}^{v})^{(k)}}{\hat{F}_{Rv}} \tag{2.72}$$

2.8 ANSYS-CFX CFD Software

Computational fluid dynamics (CFD) can be applied using commercially available software or using computer codes which are written in MATLAB, FORTRAN, etc. For this study ANSYS-CFX 11.0 was used to study the interaction of the sign support structure with a simulated natural wind gust.

ANSYS-CFX is capable of modeling steady state and transient flows, laminar and turbulent flow, heat transfer and thermal radiation etc. Like any other CFD software, ANSYS-CFX has three main elements: pre-processor, solver, and post-processor. Figure 2-13 shows these elements and what they do.

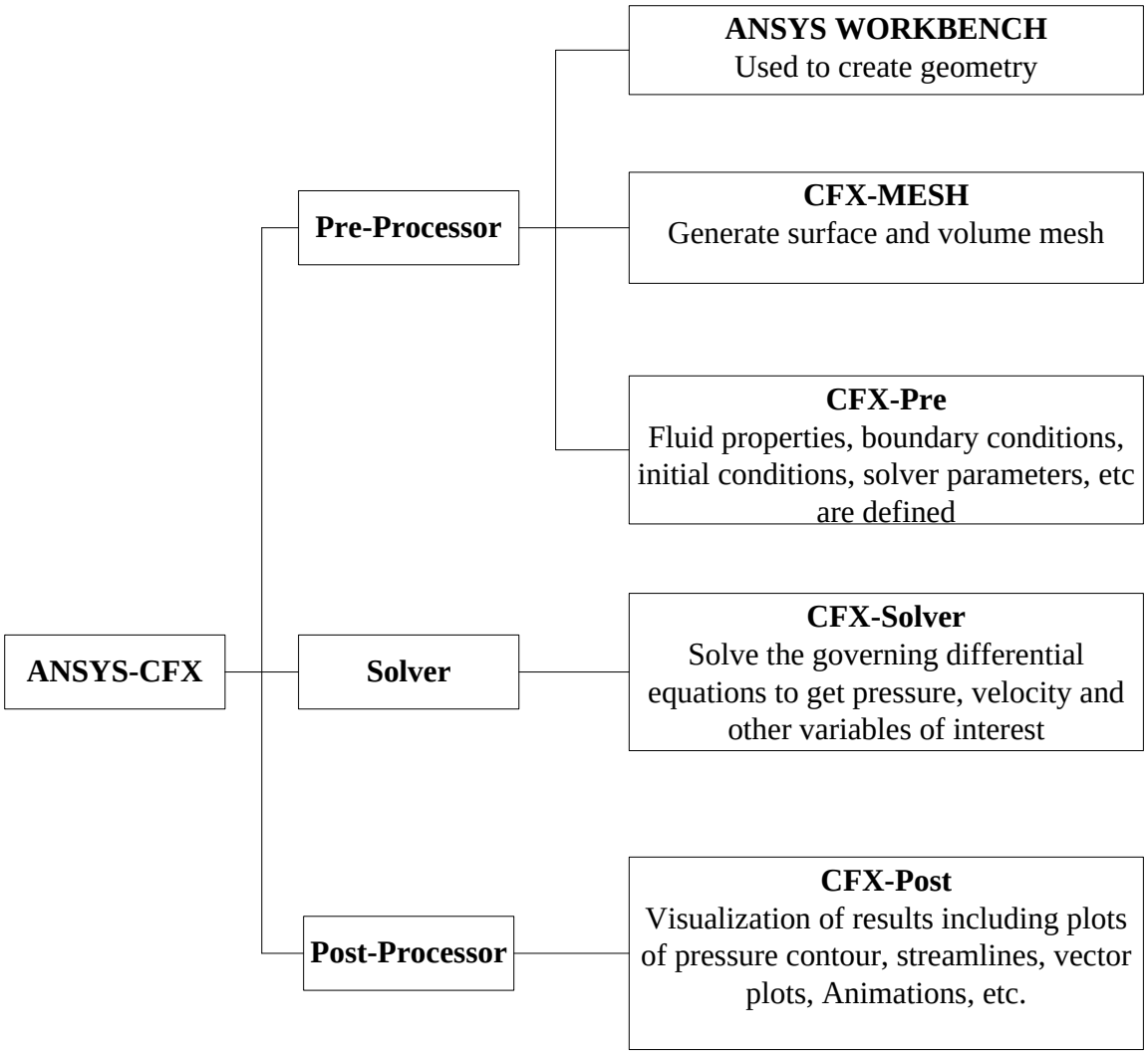

Figure 2-13: Elements of ANSYS

The pre-processing uses ANSYS WORKBENCH, CFX-Mesh, and CFX-Pre to execute different tasks. Creation of geometry is the first task which is done on ANSYS WORKBENCH. The geometry is then taken to CFX-Mesh to generate a surface and volume mesh. The final task of the pre-processing section is performed on CFX-Pre involves defining boundary conditions, assigning fluid properties, and defining solver parameters. Once the pre-processing is done, CFX-Solver starts solving the governing differential equation to get the variable of interest i.e. pressure and velocity. The results are then processed in CFX-Post to get visualization of the results including plots of pressure contours, vector plots, animations, etc.

CHAPTER III

LOADING ON SIGN SUPPORT STRUCTURES

3.1 Introduction

Cantilever sign support structures are susceptible to fatigue cracks caused by numerous cycles of wind and other loads. As these structures are usually placed on major highways and roadways there is a widespread concern regarding their reliability. In rare cases, cantilever sign support structures have failed, crashing into the roadway and presenting a hazard to the travelling public (Kaczinski et al, 1998).

According to the fourth edition of the *Standard Specifications for Structural Supports for Highway Signs, Luminaries, and Traffic Signals* (AASHTO, 2001), "in order to avoid large-amplitude vibrations and to preclude the development of fatigue cracks in various connection details and at other critical locations", cantilever and non-cantilever structures should be designed to resist four different limit states of loading. These are:

1. Galloping,
2. Vortex shedding,
3. Truck-induced gust, and
4. Natural wind gust.

3.2 Galloping

Galloping is characterized by large amplitude, resonant oscillations in a plane normal to the direction of wind flow. Sign support structures with horizontal attachments are most susceptible to galloping induced loading. The sign support structure member itself is not the cause of galloping, but rather it is the attachment to the horizontal cantilever arm such as signs and traffic signals. The susceptibility of cantilevered support structures to galloping depends on the geometry of the attachment, orientation of the attachments, and wind direction. Galloping-induced oscillations mainly occur in flexible, lightly damped structures with non-symmetrical cross sections. For instance, sign supports which are circular cylinders are not susceptible to galloping-induced vibration as they have symmetrical cross sections.

AASHTO requires overhead cantilevered sign and traffic signal support structure to be designed for galloping-induced cyclic loads by applying an equivalent static shear pressure vertically to the frontal area of the sign and traffic signal attachment. The magnitude of this vertical shear pressure is determined by:

$$P_G = 1000.I_F \quad \text{(Pa)} \tag{3.1}$$

$$P_G = 21.I_F \quad \text{(Psf)} \tag{3.2}$$

3.3 Vortex Shedding

A structural element that is exposed to a steady and uniform flow will shed vortices in a wake behind the element in a pattern commonly known as Von Karman vortex shedding. Resonant (large amplitude vibration) oscillation is produced when the vortex shedding frequency approaches the natural frequency of the structure, in most cases the first mode.

Vortex shedding is prevalent in non-tapered cross sections which are exposed to critical wind velocity less than 20m/s (65 fps; 45 mph). Sign support structures that are composed of tapered members are not susceptible for vortex induced vibration when tapered at least 0.0117m/m (0.14in/ft). The critical wind velocity, V_c can be calculated as:

$$V_c = \frac{f_n d}{s_n} \quad \text{(For circular sections)} \tag{3.3}$$

$$V_c = \frac{f_n b}{s_n} \quad \text{(For multisided sections)} \tag{3.4}$$

Where f_n is the first natural frequency of the structure; d and b are the diameter and flat-to-flat width of the horizontal mast armor pole shaft for circular and multi-sided cross sections respectively; and s_n is the Strouhal number. The Strouhal number shall be taken as 0.18 for circular sections, 0.15 for multisided sections, and 0.11 for square or rectangular sections.

The first mode natural frequency for simple pole structure, without mast arms, can be calculated using the following equations:

$$f_{n1} = \frac{1.75}{\pi}\sqrt{\frac{EIg}{WL^4}} \tag{3.5}$$

(Without luminaries mass)

$$f_{n1} = \frac{1.73}{2\pi}\sqrt{\frac{EIg}{WL^4 + 0.236wL^4}} \tag{3.6}$$

(With luminaries mass)

Where *W* is the weight of the luminaries, *w* is the weight of the pole per unit length, *g* is the acceleration of gravity, *L* is the length of the pole, and *I* is the moment of inertia of the pole. For tapered pole, I_{avg} is replaced for *I*, where:

$$I_{avg} = \frac{I_{top} + I_{bottom}}{2} \tag{3.7}$$

The first modal frequency of poles with mast arm (cantilever sign support structure) is determined by using finite element based modal analysis.

The equivalent static pressure for the design of vortex shedding induced loads shall be:

$$P_{vs} = \frac{0.613 V_c^2 C_d I_F}{2\beta} \quad \text{(Pa)} \tag{3.8}$$

$$P_{vs} = \frac{0.613 V_c^2 C_d I_F}{2\beta} \quad \text{(Psf)} \tag{3.9}$$

Where C_d is the drag coefficient; I_F is the importance factor; and β is the damping ratio, which is conservatively taken as 0.005.

The pressure calculated in Equations (3.8) and (3.9) are applied transversely to the poles (i.e., horizontal direction) and horizontal mast arms (i.e., vertical direction).

3.4 Truck-Induced Gust

A truck passing under a sign support structure may induce gust loads on the attachment mounted to the horizontal support of these structures. The equivalent static truck gust pressure for overhead sign and traffic signal support structures are given by:

$$P_{TG} = 1760 C_d I_F \quad \text{(Pa)} \tag{3.10}$$

$$P_{TG} = 36.6 C_d I_F \quad \text{(Psf)} \tag{3.11}$$

The pressure is applied in the vertical direction to the cantilevered horizontal support as well as the area of all signs, attachments, walk ways, and/or lighting fixtures projected on a horizontal plane.

For locations where the truck speed is less than 30m/s (65mph) the equivalent static pressure can be calculated as:

$$P_{TG} = 1760 C_d \left(\frac{V}{30 m/s}\right)^2 I_F \quad \text{(Pa)} \tag{3.12}$$

$$P_{TG} = 36.6 C_d \left(\frac{V}{65 mph}\right)^2 I_F \quad \text{(Psf)} \tag{3.13}$$

where, *V* is the truck speed in m/s (mph).

The elevation of the horizontal support and the height of the attachment above the truck affect the value of truck induced wind gust. However, the above equations for truck induced gust don't take into consideration these factors.

3.5 Natural Wind Gust

Turbulence is the inherent characteristics of natural wind gusts that cause fluctuations in wind velocity. The fluctuations in flow velocity induce fluctuation of pressure on the sign support structure which may finally induce vibration in the structure.

Analytical study of the response of cantilevered support structures subjected to random gust loads is used to develop the expression to calculate the equivalent static natural wind gust pressure. The equivalent static natural wind gust pressure is given by:

$$P_{NW} = 250 C_d I_F \qquad \text{(Pa)} \tag{3.14}$$

$$P_{NW} = 5.2 C_d I_F \qquad \text{(Psf)} \tag{3.15}$$

Equations (3.14) and (3.15) are used for locations with a yearly mean wind speed of 5m/s (11.2mph). For locations with higher yearly mean wind speed, V_{mean}, the equivalent static natural wind gust pressure is given by:

$$P_{NW} = 250 C_d \left(\frac{V_{mean}^2}{25}\right) I_F \qquad \text{(Pa)} \tag{3.16}$$

$$P_{NW} = 5.2 C_d \left(\frac{V_{mean}^2}{125}\right) I_F \qquad \text{(Psf)} \tag{3.17}$$

The pressure is applied to the exposed surface areas seen in an elevation view oriented perpendicular to the assumed wind gust direction.

CHAPTER IV

NATURAL WIND GUST PRESSURE

This chapter compares the equivalent static natural wind gust pressure which is calculated using AASHTO provision to the result of CFD analysis using ANSYS-CFX by considering the sign support structure discussed in Section 4.1. The analysis using ANSYS-CFX considers steady-laminar flow, transient-laminar flow and turbulent flow.

4.1 Description of the Sign Support Structure

The sign support structure under investigation shown in Figure 4-1 has horizontal and vertical members as well as a plate (i.e., sign) attached to it. All members are made from steel with modulus of elasticity 29*10^6 psi. The vertical and the horizontal members have a hollow circular cross section with thickness of 0.015 ft.

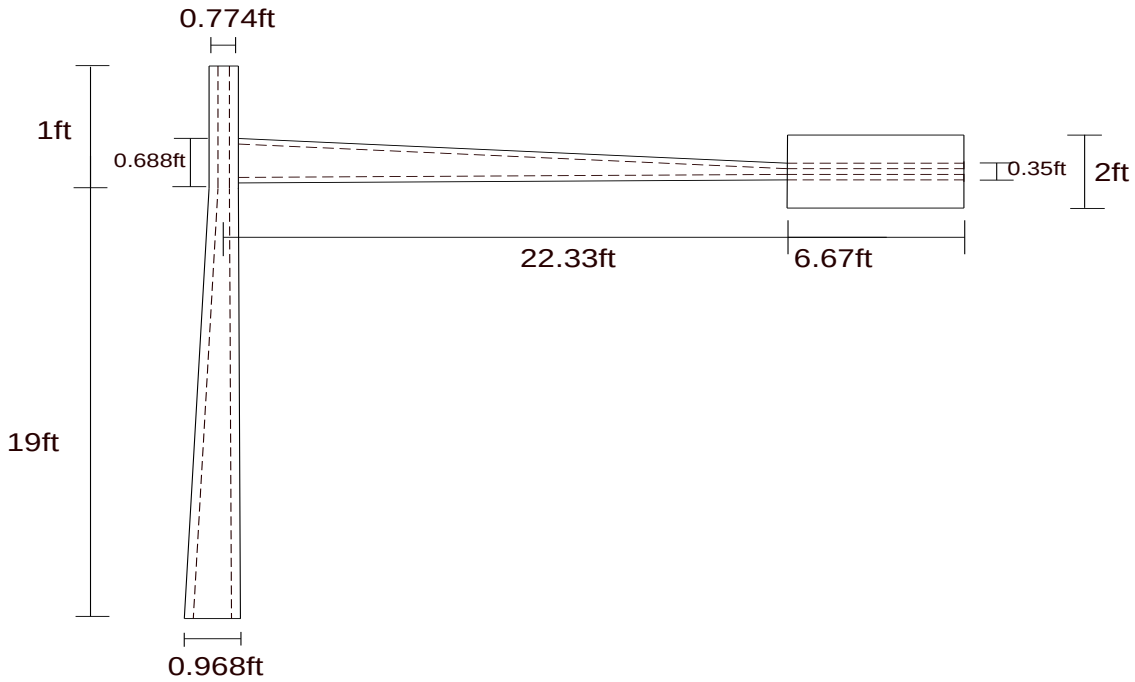

Figure 4-1: Cantilever sign support structure

The vertical member is 20 ft long. It tappers from a diameter of 0.9683ft to 0.774ft over a length of 19ft and then has a constant diameter of 0.774ft for the remaining 1 ft length. The horizontal member spans 29 ft. It tappers from a diameter of 0.688ft to 0.35ft over a length of 22.33ft and then has a constant diameter of 0.35ft for the remaining 6.67ft. The attached plate has a length of 6.67ft, width of 2ft, and thickness of 1in. The plate (or sign) is unimportant with respect to its structural stiffness and is only used to transfer the resulting wind load imparted onto the sign to the supporting structure.

4.2 Equivalent Static Natural Wind Gust Pressure Using AASHTO Provision

The provision of AASHTO for calculating the equivalent static natural wind gust pressure is derived based on a yearly mean wind speed. Equations 3.14 and 3.15, for instance, are used for areas with a yearly mean wind speed of 11.2mph. In these areas, the wind speed in some time of the year may be very low (lower than 11.2mph) and at some other time of the year may be higher (higher than 11.2mph). The fluctuation in velocity of the wind velocity also causes a fluctuation in the equivalent static pressure on the sign support. The bottom line is the provision of AASHTO for calculating the pressure is not based on a certain exact value of wind velocity (exactly 11.2mph for this case) rather it uses the yearly average value.

Calculating the equivalent static pressure for yearly mean wind speed of 5m/s (11.2mph) on the horizontal attachment of the cantilever sign support structure shown in Figure 4-1 using Equation (3.15) is provided as:

$$P_{NW} = 5.2 C_d I_F \qquad \text{(Psf)}$$

- C_d is a function of the ratio of length to width of the attachment of the sign support. $\frac{L}{W}=\frac{6.67ft}{2ft} = 3.33$, Interpolating the value of C_d from Table 3-6 of *Standard Specifications for Structural Supports for Highway Signs, Luminaries, and Traffic Signals* (AASHTO, 2001) gives 1.194.

- I_F depends on where the sign supports are installed and the degree of hazard they cause in the event of failure. For the case of the sign support under investigation it is more likely to be Category II and therefore I_F=0.85 is used from Table 11-1 of *Standard Specifications for Structural Supports for Highway Signs, Luminaries, and Traffic Signals* (AASHTO, 2001).

= 5.2*1.194*0.85 psf

= 5.28 psf

The force on the sign support F_{NW} can be calculated by multiplying the pressure with the area of the attachment (5.28 psf*2ft*6.67ft) providing 70.43lb. The force is then applied at the centroid of the horizontal attachment as provided in Section 4.3 of this study.

4.3 Equivalent Static Natural Wind Gust Pressure Using ANSYS-CFX

Time dependent and time independent laminar flow as well as time independent turbulent flows are considered for the analysis of the sign support on ANSYS-CFX.

The analysis begins by creating the geometry of the sign support structure and the computational domain on ANSYS WORKBENCH. Figures 4-2 and 4-3 show the model of the sign support structure and the computational domain which are created on ANSYS WORKBENCH. A full scale model is employed where both the computational domain and the sign support structure aren't scaled. The dimension of the computational domain is shown in Figure 4-4. Its size is limited because of the limited computational power of the computer.

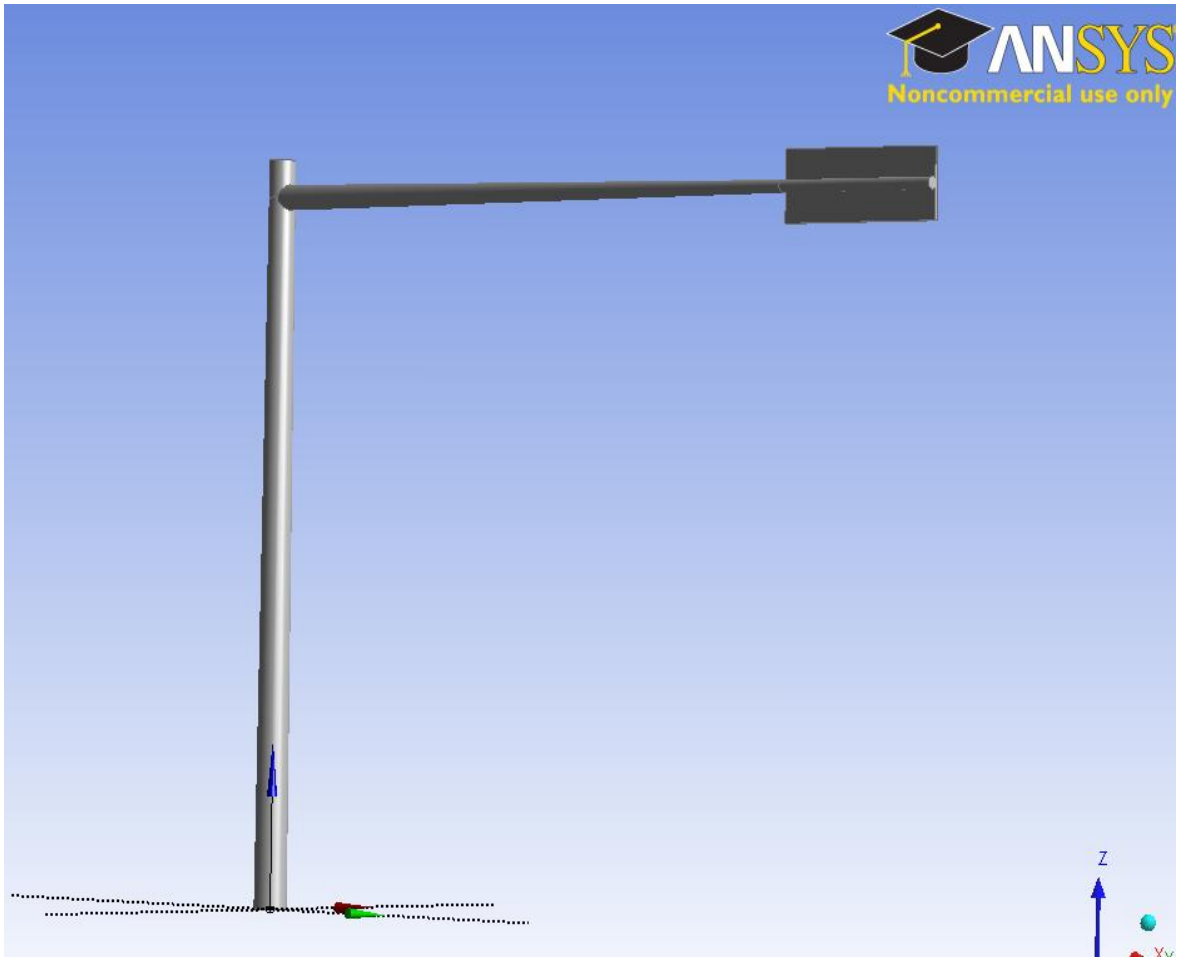

Figure 4-2: Model of the Sign Support Structure

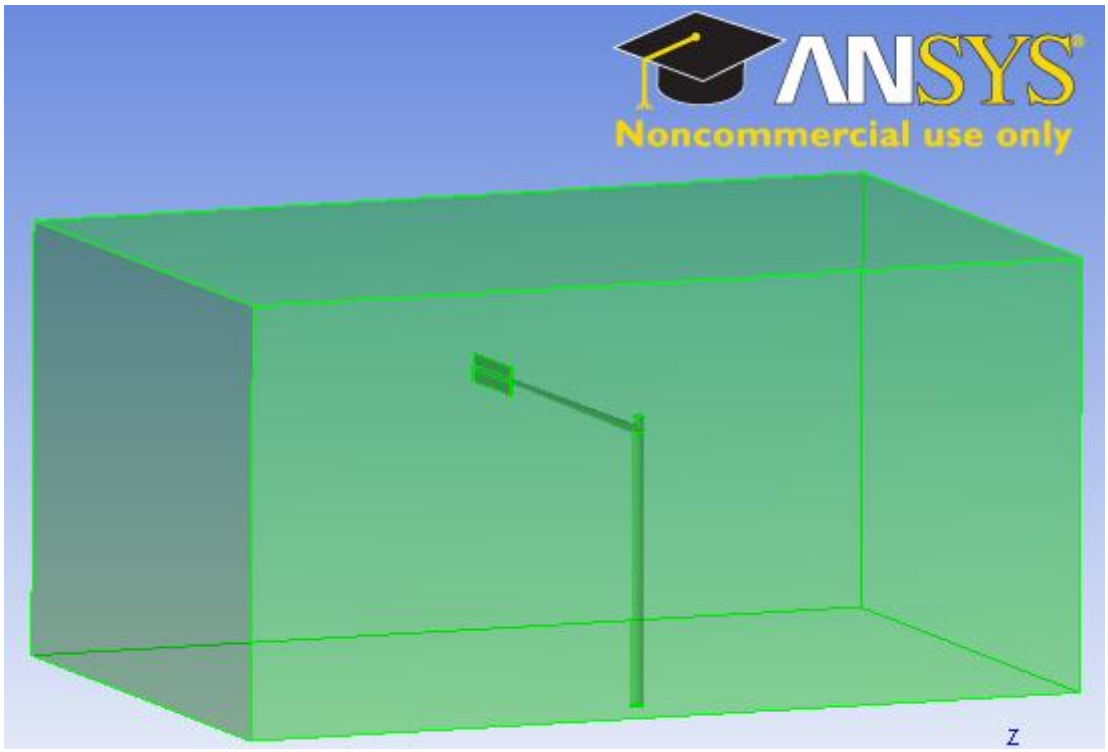

Figure 4-3: Model of the Sign Support Structure and the Computational Domain

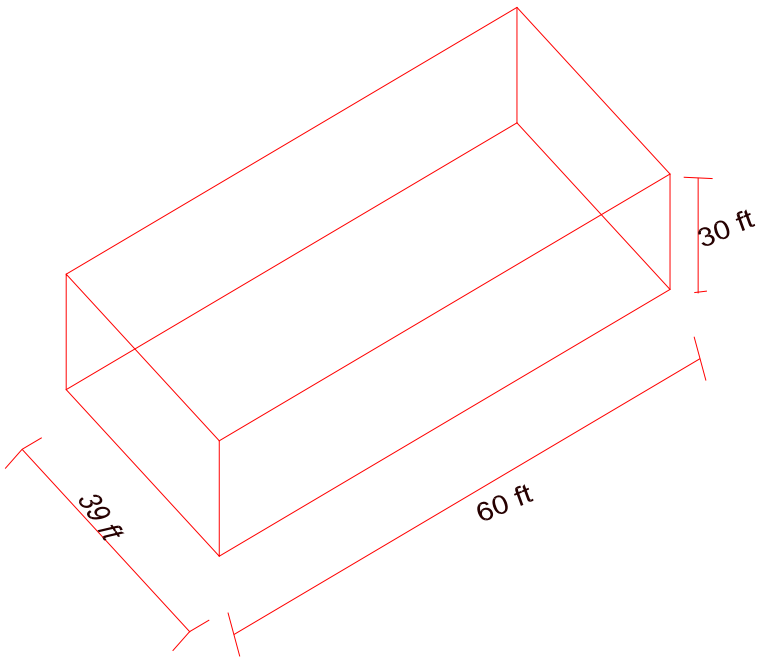

Figure 4-4: Dimension of the computational domain

After the creation of geometry, the mesh is generated by using ANSYS-CFX. An optimal mesh is utilized such that a fine mesh is generated around the sign support structure since it is expected to show variation while a coarser mesh is used in other locations.

The mesh is then taken to CFX-Pre to perform the following tasks:

- Defining material properties. Air ideal gas is used for the simulation because at standard temperature and pressure most real gases behave like ideal gases. Ideal gas deviates from real gases at lower temperatures and higher pressures as real gases undergo a transition of phase to either liquid or solid.
- Modeling the fluid flow as laminar, turbulent or transient.
- Defining as well as assigning the value of the boundary condition. A velocity of 5m/s (16.4ft/s) is assigned at the inlet (for all the cases considered). The top and the sides of the computational domain are defined as a free-slip boundary condition. In free-slip boundary conditions the velocity parallel to the wall is non-zero as there is no surface which creates shear stress to retard the flow. However, the sign support structure and the boundary condition on the lowest Z-axis is assigned a non-slip boundary condition.
- Initialize the flow by assigning a guessed value of velocity.
- Assigning of the number of iterations and the residual limit. For all the cases considered, 100 iterations and a residual limit of 10^{-5} are assigned.
- For transient flow, the total time for the simulation and time step are defined. For the current investigation a total time of 30 second is used. The time steps are 0, 1, 2, 3, 4, 8, 12, 16, 20, 24, 28, and 30 seconds.

The model is then analyzed using the CFX-Solver to solve for the variables of interest such as pressure and velocity. Finally, the results from CFX-Solver are processed in CFX-Post to generate graphics showing pressure contour, velocity vector, and streamlines, etc.

Analysis Results for Steady-Laminar Flow

Figures 4-5 to 4-8 show the output for the analysis of the sign support structure for steady-laminar flow. The pressure contour on the windward and leeward sides are shown in Figure 4-5 and 4-6, respectively. The velocity vectors on the free walls and around the sign support structure are shown in Figure 4-7 and 4-8, respectively.

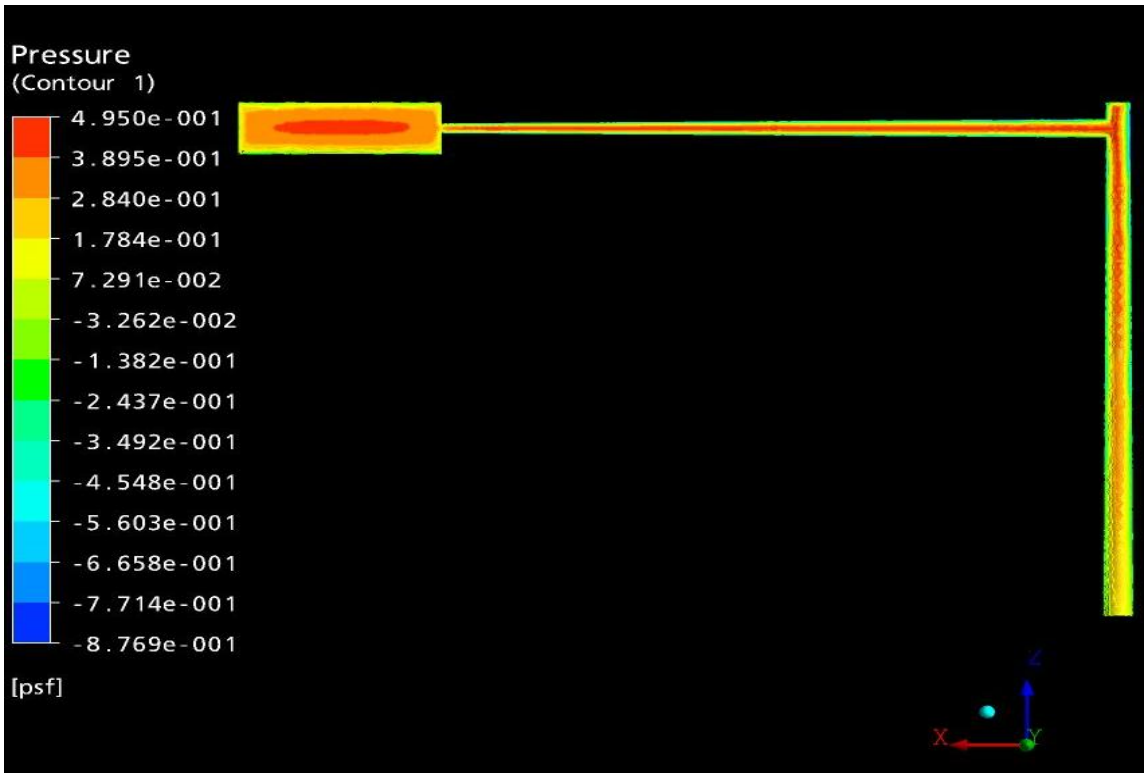

Figure 4-5: Pressure Contour on the Windward Side for Steady-Laminar Flow

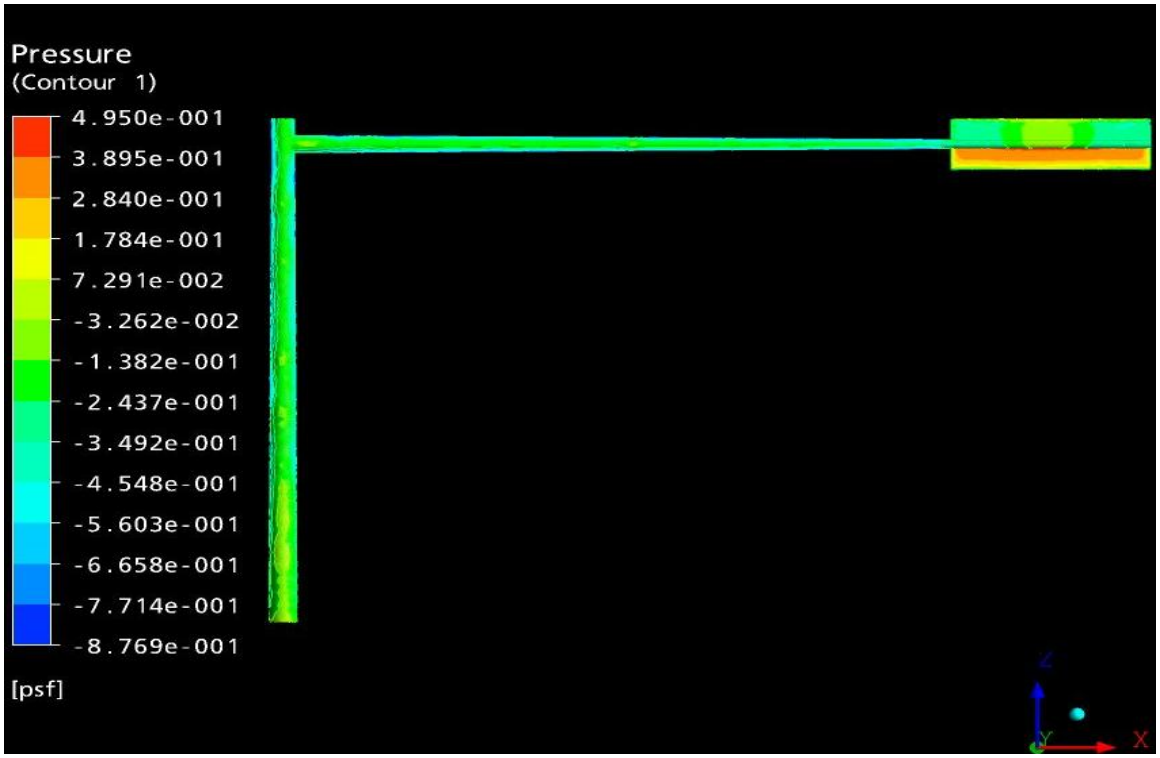

Figure 4-6: Pressure Contour on the Leeward Side for Steady-Laminar Flow

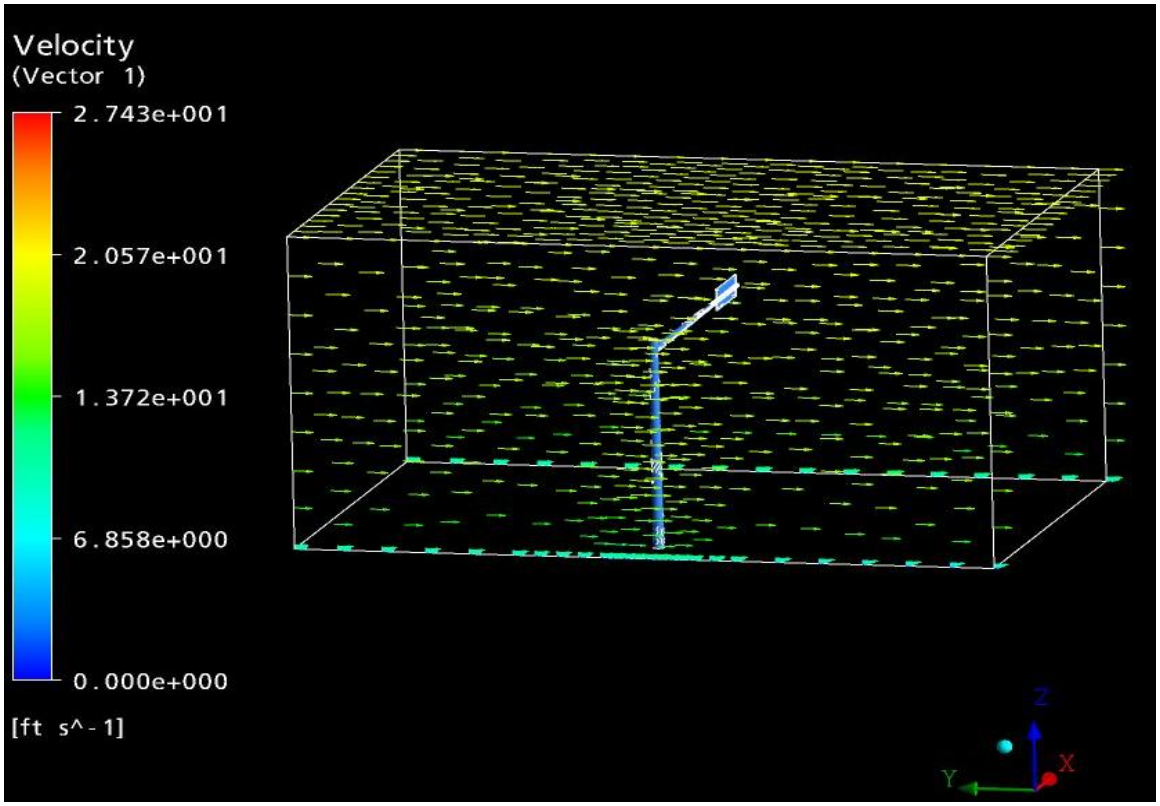

Figure 4-7: Velocity Vectors on the Free Walls

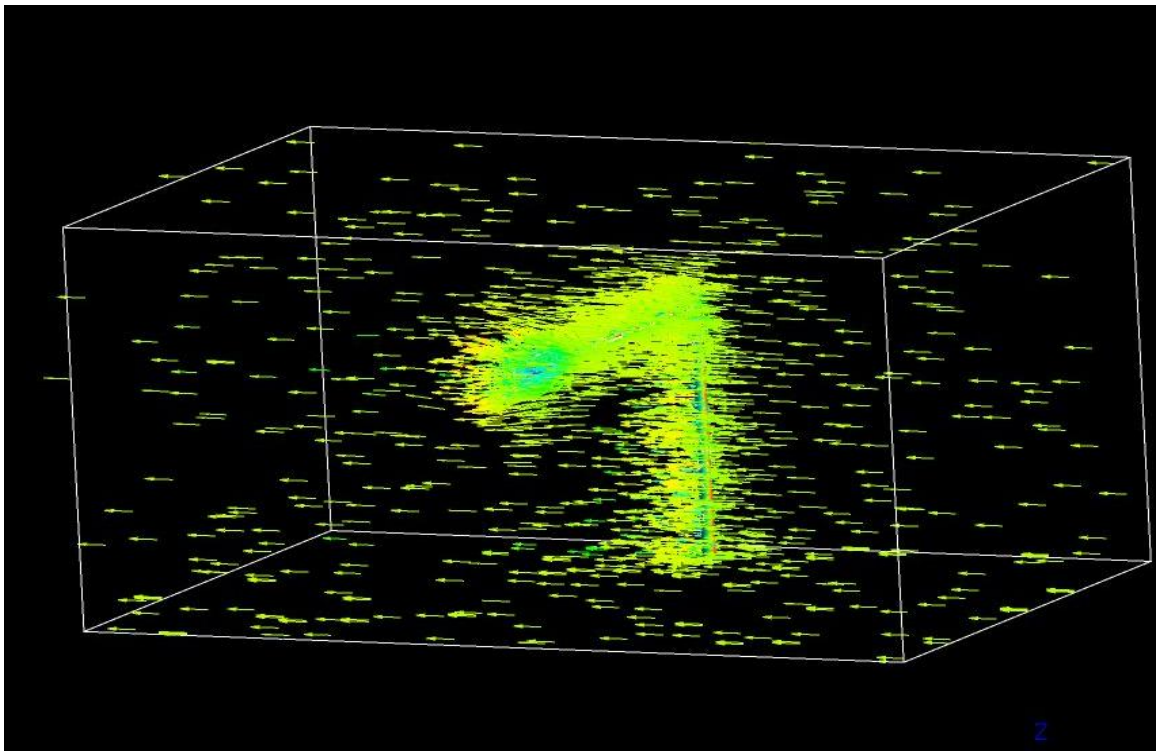

Figure 4-8: Velocity Vectors around the Sign Support

Analysis Results for Transient-Laminar Flow

To see the variation of pressure over time a graph is plotted for a point at the centroid of the horizontal attachment as shown in Figure 4-9. The pressures at different time steps are approximately equal. It can be observed that the pressure up to 12sec (within the first few time steps) is 0.326761psf. After a number of time steps have been determined, the laminar flow "smoothes" into a uniform flow and the pressure attains a constant value of 0.326763psf.

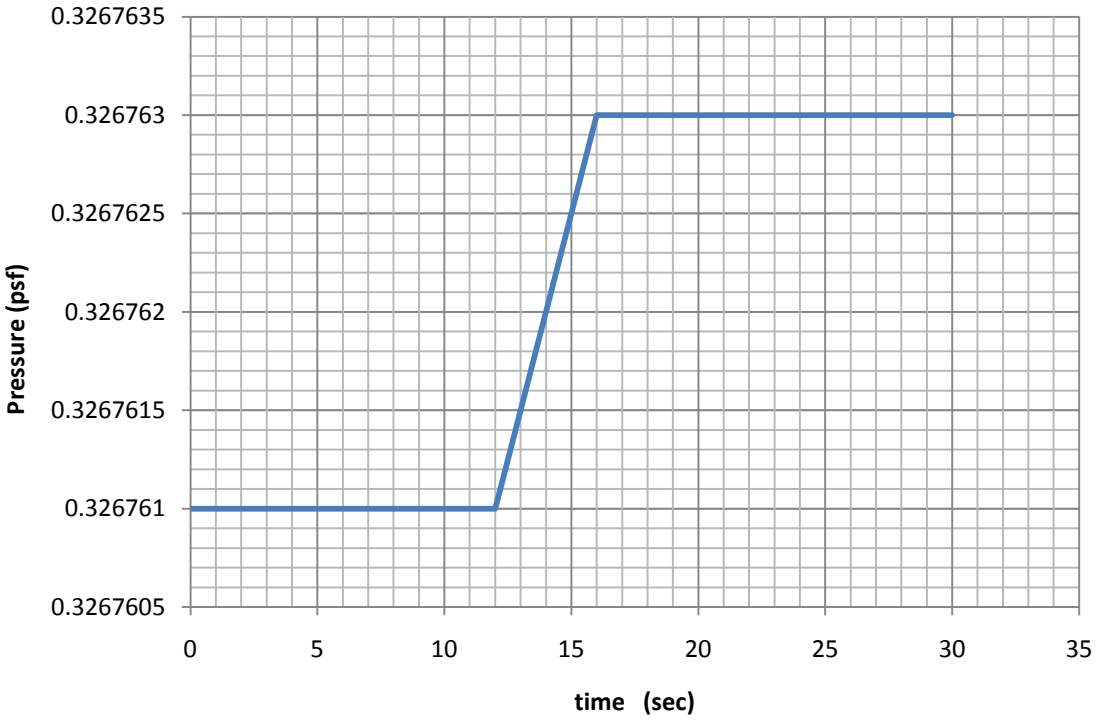

Figure 4-9: Pressure vs. time for a point at the centroid of the horizontal attachment

Figures 4-10 and 4-11 show the pressure contour on the windward and leeward side of sign support structure for transient-laminar flow. The pressure contour didn't show big variation for different time steps. Hence, the result at the beginning of the time steps is shown in the following figures.

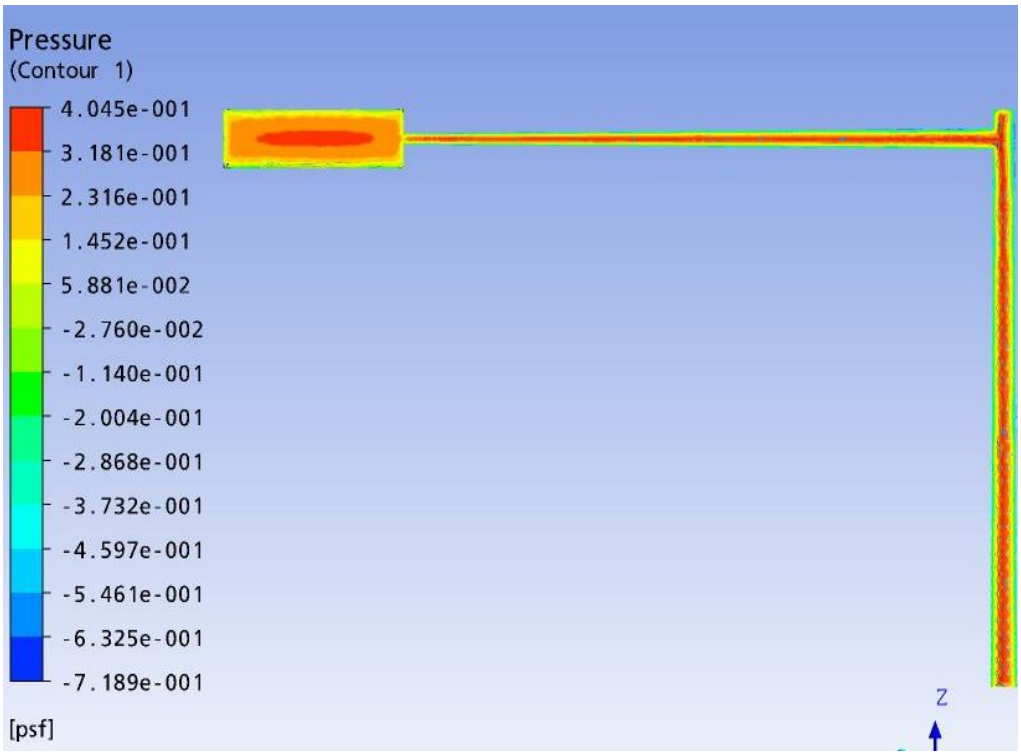

Figure 4-10: Pressure Contour on the Windward Side for Transient-Laminar Flow

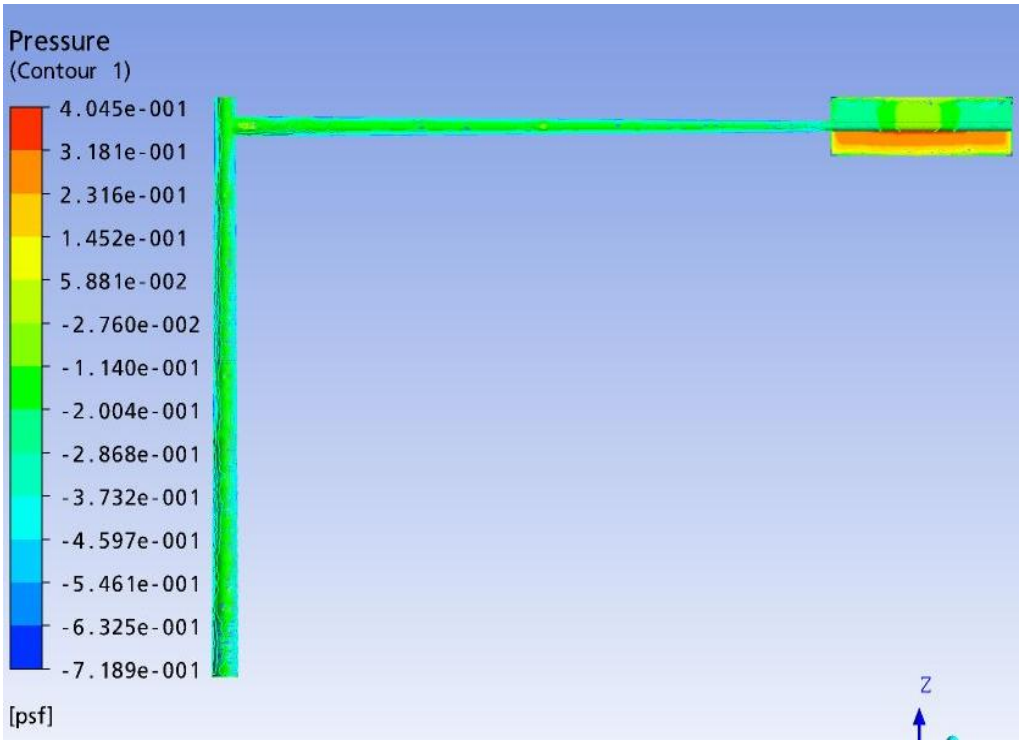

Figure 4-11: Pressure Contour on the Leeward Side for Transient-Laminar Flow

Analysis Results for Steady State Turbulent Flow

Figures 4-12 and 4-13 show the pressure contour on the windward and leeward side of sign support structure for turbulent flow.

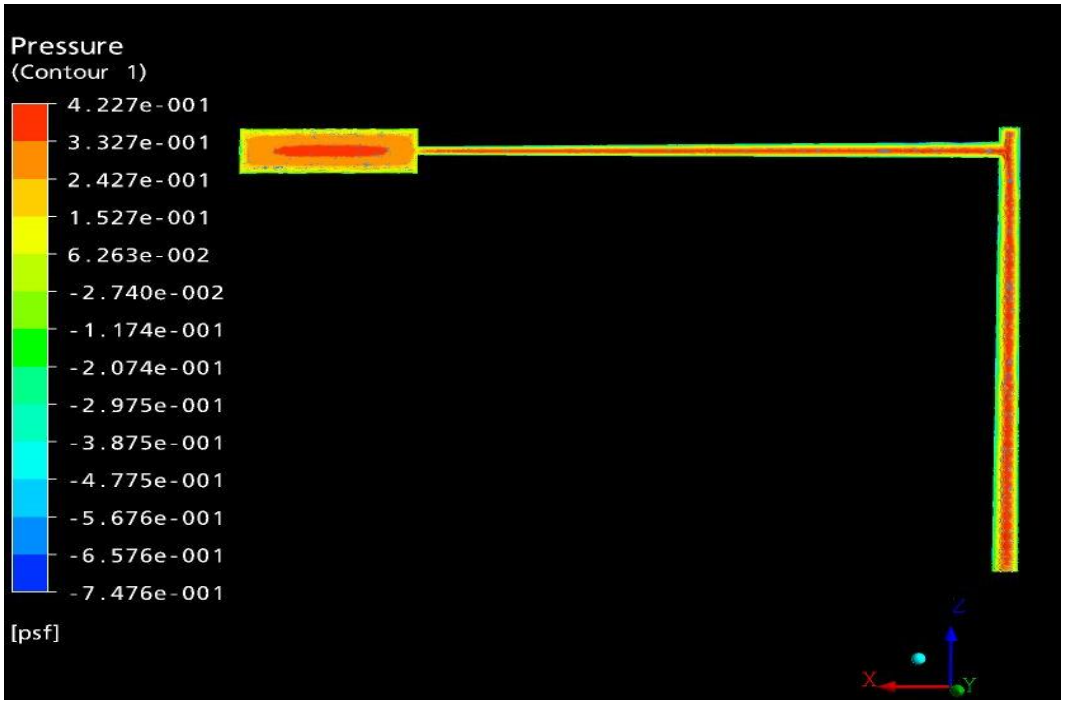

Figure 4-12: Pressure Contour on the Windward Side for Turbulent Flow

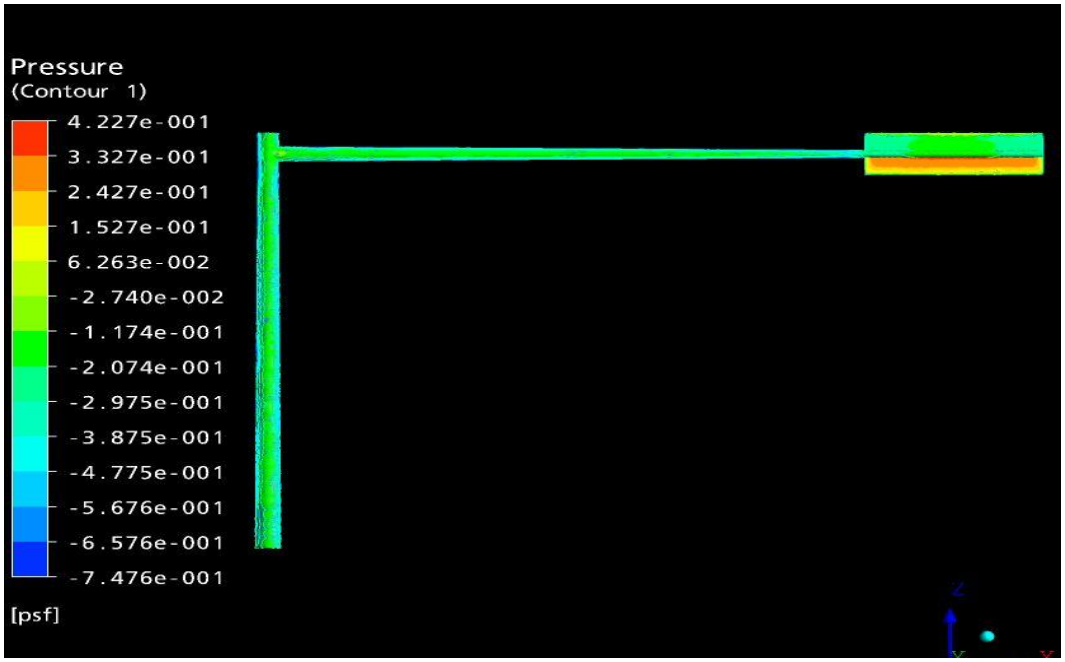

Figure 4-13: Pressure Contour on the Leeward Side for Turbulent Flow

The pressure on the attachment of the sign support structure isn't uniformly distributed. In order to perform static analysis to calculate the stress, the area is subdivided approximately (each division of the areas have approximately the same values of pressure) and then the force on each division is found by multiplying their area with their respective pressure. Summing up the force both on the windward and leeward side gives the resultant force. The resultant force is then applied at the centroid to get the stress. The following table shows the resultant force on the attachment of the sign support structure for different scenario of flow cases:

Flow Condition	Resultant Force
Steady-Laminar flow	4.22 lb
Transient-Laminar flow	3.53 lb
Steady-Turbulent flow	3.80 lb

Table 4-1: Resultant Forces

4.4 Equivalent Static Analysis

The static analysis is determined using a structural analysis program, STAAD Pro 2007. The resultant forces which are determined using AASHTO provision as well CFD analysis are applied at the centroid of the horizontal attachment of the sign support structure to get the bending moment due to each load. Figures 4-14 to 4-17 show the result of the equivalent static analysis for the different scenarios of CFD analysis as well as for the load from AASHTO provision.

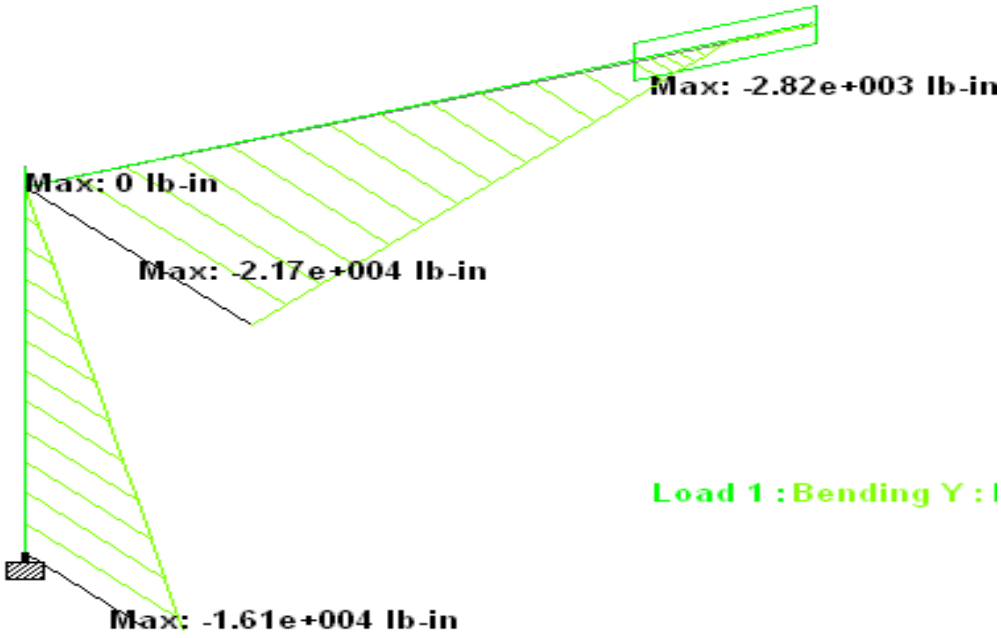

Figure 4-14: Bending moment on sign support from AASHTO provision

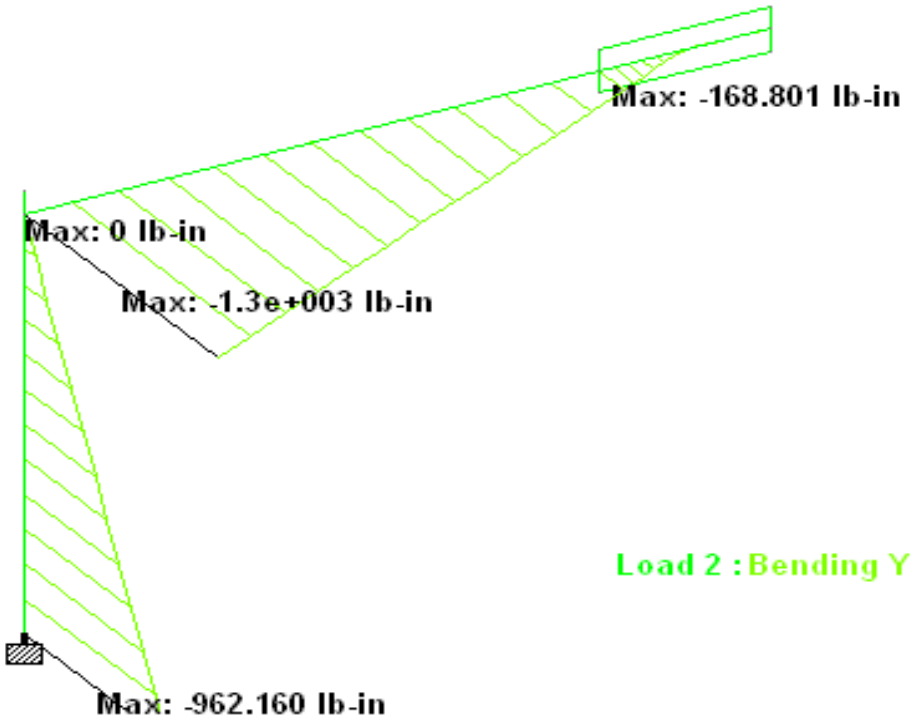

Figure 4-15: Bending moment on the sign support for steady-laminar flow

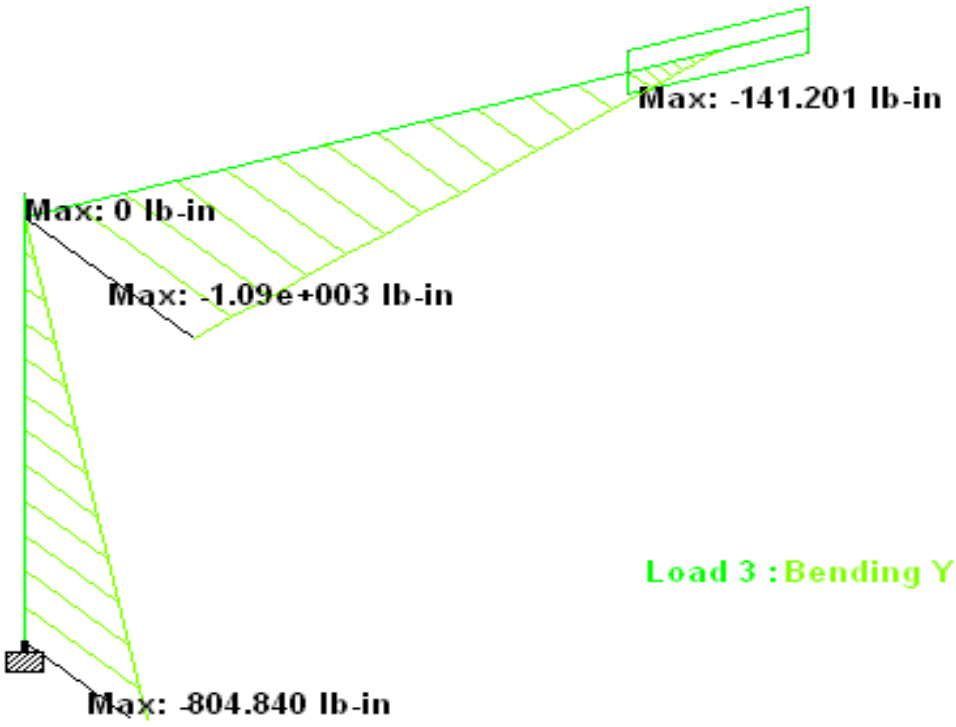

Figure 4-16: Bending moment on the sign support for transient-laminar flow

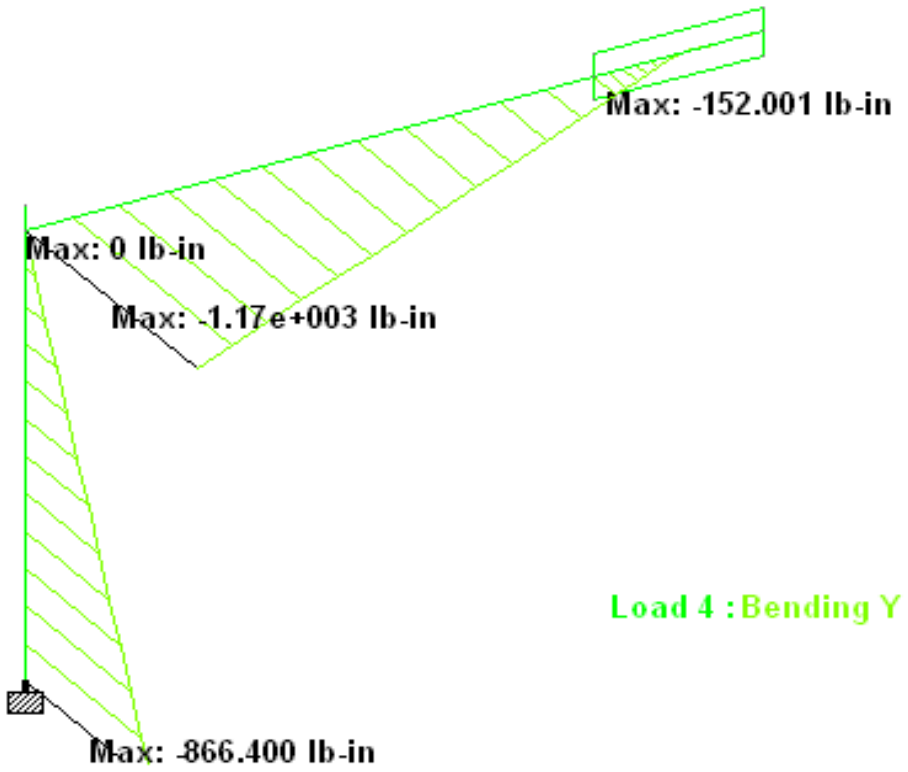

Figure 4-17: Bending moment on the sign support for steady-turbulent flow

4.5 Summary

The highest stress concentration, which is mainly bending, is observed at the base as well as at the connection between the horizontal and vertical member of the sign support structure. Table 4-2 shows the comparison of bending stress at the two locations from CFD analysis and AASHTO provision.

Type of flow/provision	Moment at the base (lb.in)	Moment at the connection (lb.in)
Steady-laminar flow	962.16	1,300
Steady-Turbulent flow	866.4	1,170
Transient-laminar flow	804.84	1,090
AASHTO provision	16,100	21,700

Table 4-2 Comparison of bending moment at the critical locations

As seen from Table 4-2, the bending stress from the AASHTO provision is much greater than the bending stress from the CFD analysis. As it is explained in Section 4.2, AASHTO considers a yearly mean wind speed where as the CFD analysis takes into consideration a one-time natural wind gust. After running the model for different wind velocities, it is found that the pressure on the structure for 22.35m/s (50mph) wind gust in ANSYS-CFX gives approximately an equal value of stress with the value of the wind gust pressure calculated using AASHTO provision for a yearly mean wind speed of 5m/s (11.2mph). Figures 4-18 and 4-19 show the pressure on the windward and leeward side for a wind gust velocity of 22.35m/s (50mph).

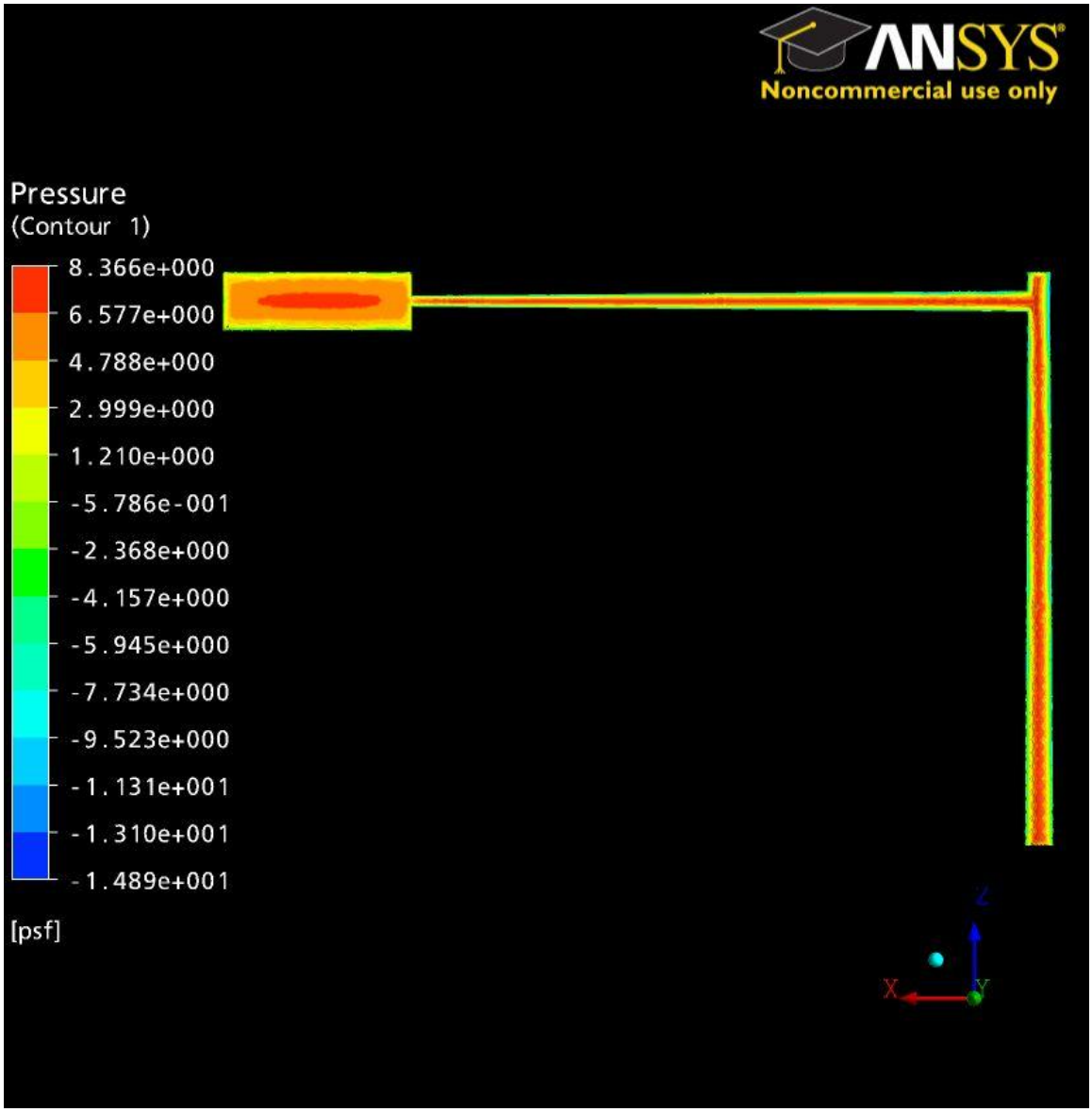

Figure 4-18: Pressure Contour on the Windward Side for 50 mph wind gust (Steady-Laminar Flow)

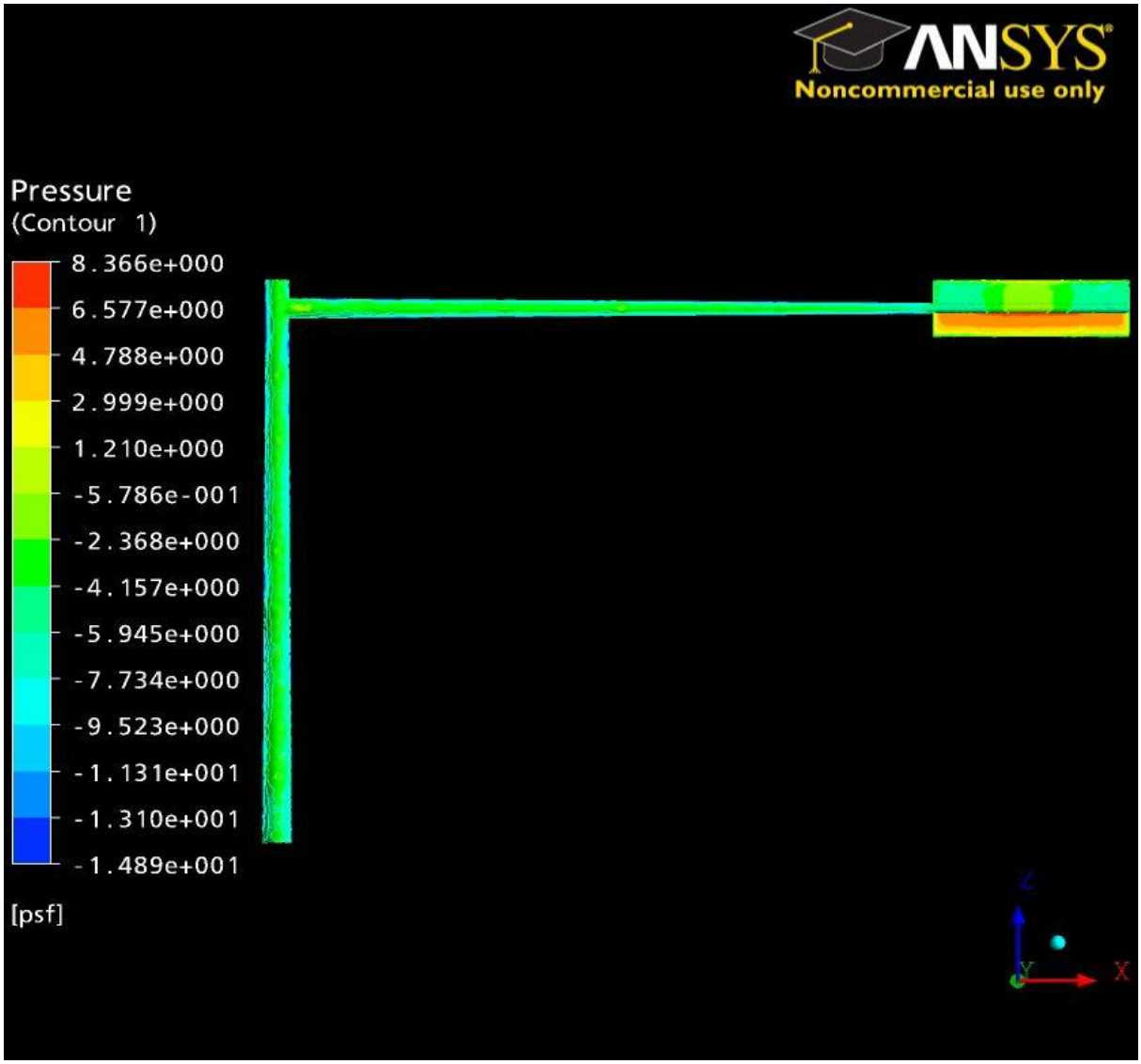

Figure 4-19: Pressure Contour on the Leeward Side for 50 mph wind gust (Steady-Laminar Flow)

Calculating the resultant force on the horizontal attachment for a 50mph wind gust gives 71.5 lb. It can be observed from Figure 4-20 the bending stress due to a 22.35m/s (50mph) wind gust is approximately equal to the bending stress calculated using AASHTO provision (Figure 4-14) for 5m/s (11.2mph).

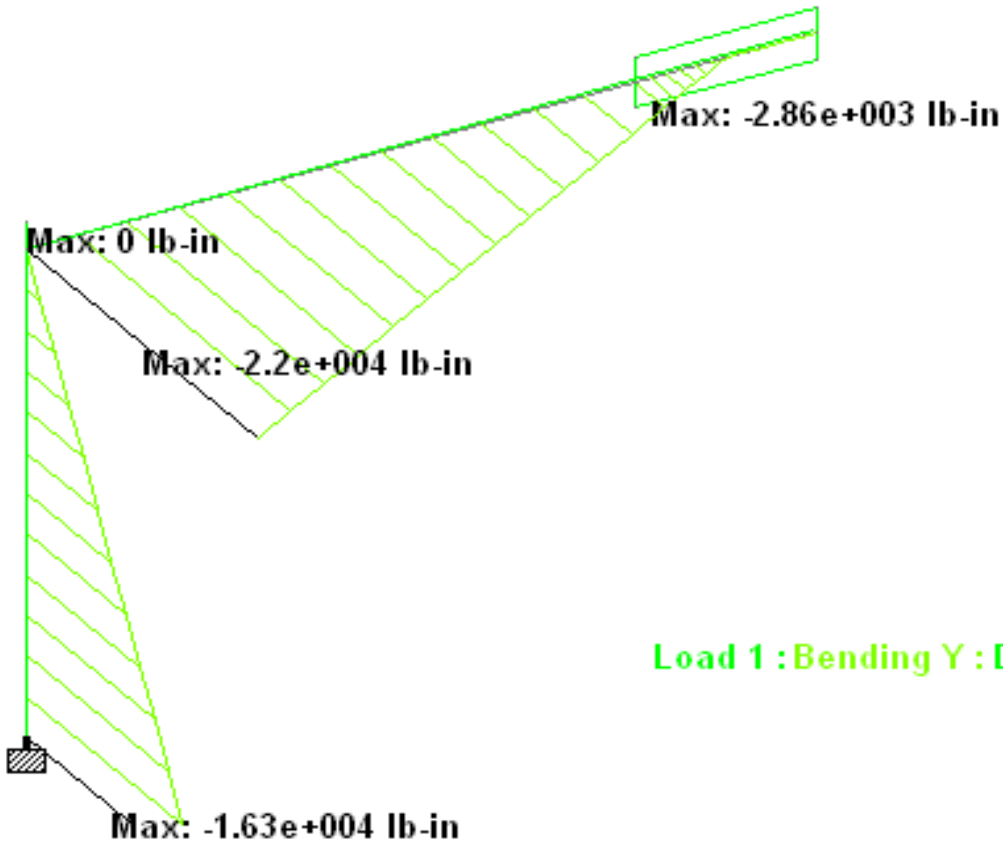

Figure 4-20: Bending moment on the sign support for 50mph wind gust

The second observation from the result is that the bending stress of steady laminar flow is greater than that of turbulent (steady) flow. This is because, in the case of laminar flow the blowing wind acts at all points at the same time where as in turbulent flow all parts of the structure will not be under the effect of the blowing wind at the same time.

The final observation from the result is the bending stress of transient-laminar flow is less than that of steady-laminar flow. This is because in transient-laminar flow the sign support is analyzed for limited time (30sec). If the flow is analyzed for infinite time and if the computational power of the computer is unlimited the result of transient-laminar flow will be equal to the value of steady-laminar flow.

CHAPTER V

CONCLUSION AND RECOMMENDATIONS

Computational fluid dynamics (CFD) has been used in different disciplines of science and engineering including civil engineering. The current research demonstrates its practical application in structural engineering. The study achieved the entire stated goal in Chapter One. First it is able to develop the theoretical background of CFD. Second, it compares the stress on the cantilever sign support structure which is determined from AASHTO provision to that of CFD analysis. Finally it is able to show the application of CFD to civil engineering infrastructure.

The theoretical background that included the governing equation of fluid flow, methods of discretization, discretization of the Navier-Stokes equation, solution algorithms for steady and unsteady flows as well as iterative convergence and residual are explained in Chapter 2. Chapter 3 presented the provision of AASHTO for design of sign support structure. The four limit states of loading (galloping, vortex shedding, truck induced gust and natural wind gust) were discussed.

Chapter 4 made comparisons of bending stress from the AASHTO provisions to that of CFD analysis using ANSYS-CFX for a wind speed of 5m/s (11.2mph). The comparison of stress is performed at locations where high stress concentrations are expected such as at the base and at the connection between the horizontal and vertical member of the sign support structure. The result showed that the bending stress from AASHTO provision is much greater than bending stress from CFD analysis. The reason behind this result is that AASHTO considers a yearly mean wind speed where as the CFD analysis takes into consideration only a one time wind gust. Further analysis is done to find out the value of a wind gust that corresponds for a yearly mean wind speed of 5m/s (11.2mph). It is found that the pressure on the structure for 22.35m/s (50mph) wind gust in ANSYS-CFX gives approximately the same value of stress with the value of the wind gust pressure calculated using AASHTO provision for a yearly mean wind speed of 5m/s (11.2mph).

However, the analysis on ANSYS-CFX has the following limitations:

- Wind from only one direction is considered at the inlet of the computational domain.
- The velocity of wind is assigned as a constant value of 5 m/s at all heights in the inlet.

However, the velocity of wind varies with height. To take this into account the logarithmic or power law can be used to define the variation of wind velocity with height for a fully-developed wind flow describing its mean wind velocity with respect to height.

- The size of the computational domain considered for analysis is small. This is due to limited computational power of the computer.
- The force on the sign support structure is calculated by approximately dividing the area of the attachment.

Based on the work done here, future studies may be able to validate the provision of AASHTO for calculating the equivalent static natural wind gust pressure by incorporating the following points:

- Taking into consideration records of wind velocity data for many years.
- Larger size computational domain that takes into account the interference from adjoining structures.
- Wind velocity from different directions.
- Assigning velocity which accurately describes the variation of wind velocity with respect to height.
- Using a more accurate method to calculate the force on the sign support.

REFERENCES

[1] AASHTO (2001), Standard Specifications for Structural Supports for Highway Signs, Luminaires, and Traffic Signals, American Association of State Highway Transportation Officials.

[2] Ansys (2006), "ANSYS-CFX Tutorials" , ANSYS Europe ltd.

[3] Ansys (2006), "ANSYS WORKBENCH Tutorials" , ANSYS Europe ltd.

[4] T. J. Chung (2002), "Computational Fluid Dynamics", Cambridge University Press, First Edition.

[5] R. J. Dexter, M.R. Kaczinski, and J. P. Van Dien (1998), "NCHRP Report 412: Fatigue-Resistant Design of Cantilevered Signal, Sign and Light Supports", National Academy Press.

[6] R. J. Dexter and J. P. Van Dien (2002), "NCHRP Report 469: Fatigue-Resistant Design of Cantilevered Signal, Sign and Light Suppors", National Academy Press.

[7] J. H. Ferziger and M. Peric (2002), "Computational Methods for Fluid Dynamics", Springer-Verlag, Third Edition.

[8] Jennifer A. Kacin (2009), "Fatigue Life Estimation of Highway Sign Structure", University of Pittsburgh.

[9] C. Kleinstreuer (1997), "Engineering Fluid Dynamics, an Interdisciplinary Systems Approach", Cambridge University Press, First Edition.

[10] H. K. Versteeg and W. Malalasekera (2007), “An Introduction to Computational Fluid Dynamics”, Pearson Education Limited, Second Edition.

[11] WSMV (2008), “TDOT TO INSPECT SIGNS AFTER COLLAPSE”, http://www.wsmv.com/news/16813368/detail.html, Accessed on MAY 8, 2010.

[12] O. C. Zienkiewicz and K. Morgan (2006), “Finite Elements & Approximations”, Dover Publications, Inc

VITA

Eyosias Beneberu

Candidate for the Degree of

Master of Science

Thesis: Computational Fluid Dynamics for Civil Engineering Infrastructure

Major Field: Civil Engineering

Biographical:

Personal Data:
Woreilu/Ethiopia

Education:
Bachelor of Science in Civil Engineering (2007)

Completed the requirements for the Master of Science in Civil Engineering at Oklahoma State University, Stillwater, Oklahoma. (2010)

Experience:

- Teaching Assistant at Oklahoma State University, Stillwater, Oklahoma
- Research Assistant at Natural Hazard Research Laboratory, Oklahoma State University, Stillwater, Oklahoma
- Structural Engineer at ZIAS Design International, Addis Ababa, Ethiopia
- Summer Internship at Ethiopian Telecommunication Corporation, Addis Ababa, Ethiopia

Professional Memberships:

- Engineers without Borders USA (EWB-USA)
- American Society of Civil Engineers (ASCE)
- American Concrete Institute (ACI)
- American Institute of Steel Construction (ASCE

Name: Eyosias Beneberu Date of Degree: July, 2010

Institution: Oklahoma State University Location: Stillwater, Oklahoma

Title of Study: Computational Fluid Dynamics for Civil Engineering Infrastructure

Pages in Study: 66 Candidate for the Degree of Master of Science

Major Field: Civil Engineering

Scope and Method of Study:

The research has three main objectives. The first objective is to develop the theoretical background of CFD. The second objective is to compare the result of wind fatigue design load on cantilever sign support structure specifically for natural wind gust using computational fluid dynamics (CFD) with the result from the AASHTO provision which is derived by considering the yearly mean wind speed. The final objective is to show the application of CFD in civil engineering.

Findings and Conclusions:

The bending stress at the critical locations i.e. at the base and at the connection between the horizontal and vertical member are considered to compare the result of AASHTO provision to that of CFD analysis. The results shows that the bending stress from AASHTO provision is much greater than the bending stress form the CFD analysis. This is because AASHTO considers a yearly mean wind speed where as the CFD analysis take into consideration a onetime natural wind gust. After running the model for different wind velocity, it is found that the pressure on the structure for 22.35m/s (50mph) wind gust in ANSYS-CFX gives approximately equal value of stress with the value of the wind gust pressure calculated using AASHTO provision for a yearly mean wind speed of 5m/s (11.2mph).

ADVISER'S APPROVAL: Dr. Jonathan S. Goode